https://doi.org/10.5194/egusphere-2025-23
Preprint. Discussion started: 21 January 2025

Incorporation of multi-phase halogen chemistry into Community Multiscale Air Quality (CMAQ) model

Kiyeon Kim[1], Chul Han Song[1*], Kyung Man Han[1], Greg Yarwood[2], Ross Beardsley[2], and Saewung Kim[3]

1. School of Earth Science and Environmental Engineering, Gwangju Institute of Science and Technology (GIST), Gwangju 61005, Republic of Korea
2. Ramboll, Novato, CA 94945, USA
3. Department of Earth System Science, University of California, Irvine, CA, USA

Shortened title: Multi-phase halogen chemistry

***Corresponding author:** Chul Han Song (chsong@gist.ac.kr)

https://doi.org/10.5194/egusphere-2025-23
Preprint. Discussion started: 21 January 2025

Abstract

Recent studies have revealed that halogen radicals (Cl, Br, and I) significantly influence atmospheric oxidation capacity, affecting O_3 formation or destruction. However, understanding of halogen chemistries remains limited. To better investigate atmospheric halogen chemistries, we incorporated halogen processes into the Community Multi-scale Air Quality (CMAQ) model: (i) emissions of Cl_2, HCl, Br_2, and HBr from anthropogenic sources, and Br_2, I_2, HOI, and halocarbons from natural sources; and (ii) 177 multi-phase halogen reactions. After developing the model, we examined its performance against observed data. The results demonstrated significant improvements in simulating observed nitryl chloride ($ClNO_2$) mixing ratios at supersites. The index of agreement (IOA) improved from 0.41 to 0.66, and the mean bias (MB) decreased from -159.36 ppt to -25.07 ppt. These improvements were driven by four atmospheric key reactions: (i) $ClO + ClO \rightarrow Cl_2$; (ii) $HOBr + Cl^- \rightarrow BrCl$; (iii) different parameterization of γ_{N2O5}; and (iv) $2NO_2 + Cl^- \rightarrow ClNO + NO_3^-$. We then examined the net O_x production rate ($P(O_x)$), which increased from 3.08 ppb/h to 3.33 ppb/h on land and decreased from 0.21 ppb/h to 0.07 ppb/h over ocean in the presence of halogen radicals. Further analysis of the impacts of halogen processes on key atmospheric species revealed that levels of OH, HCHO, and NO_x increased by ~0.007 ppt (5.5%), ~0.03 ppb (1.6%), and ~0.29 ppb (2.9%), respectively, while levels of HO_2 and VOCs decreased by ~0.45 ppt (5.3%) and ~0.71 ppb (5.9%), respectively.

Keywords: Halogen chemistry; Anthropogenic halogen emission; Nitryl chloride ($ClNO_2$); Net O_x production ($P(O_x)$)

https://doi.org/10.5194/egusphere-2025-23
Preprint. Discussion started: 21 January 2025

1. Introduction

Atmospheric oxidants, such as OH, NO_3, and O_3, play a significant role in atmospheric chemistry. These oxidants react with volatile organic compounds (VOCs), leading to the formation of peroxyl radicals (RO_2), which, in turn, influences the O_3 formation. They also contribute to the formation of secondary organic and inorganic aerosols. Meanwhile, halogen radicals (such as Cl, Br, and I) also serve as oxidants in the atmosphere, affecting the oxidation capacity through various reactions (R1 – R4; see below) (Simpson et al., 2015; von Glasow and Crutzen, 2003; Fan and Li, 2022).

$$\text{X (Cl, Br, and I)} + \text{VOC} \rightarrow RO_2 \quad \text{(R1)}$$

$$RO_2 + NO \rightarrow NO_2 + RO \quad \text{(R2)}$$

$$HO_2 + NO \rightarrow NO_2 + OH \quad \text{(R3)}$$

$$NO_2 \xrightarrow{hv} O^{3p} + O_2 \xrightarrow{M} O_3 \quad \text{(R4)}$$

$$X + O_3 \rightarrow XO + O_2 \quad \text{(R5)}$$

$$XO + HO_2 \rightarrow HOX + O_2 \quad \text{(R6)}$$

$$HOX \xrightarrow{hv} X + OH \quad \text{(R7)}$$

These radicals can also make substantial impacts on the O_3 loss via reactions (R5) – (R7) (Saiz-Lopez et al., 2012; Sarwar et al., 2015; Simpson et al., 2015). Given their roles in both the O_3 formation and destruction, a comprehensive understanding of atmospheric halogen chemistries is essential for accurately assessing the oxidative potentials of the atmosphere.

In this context, several studies attempted to incorporate chlorine chemistry into chemical-transport models (e.g., Yi et al., 2021; Sarwar et al., 2012; Qiu et al., 2019a and b). Specifically, Qiu et al. (2019a) reported that heterogeneous reactions involving reactive chlorine species can increase O_3 levels by approximately 20%. Moreover, Liu et al. (2018) found that the mixing ratios of O_3 increased by ~7.7 ppbv when anthropogenic chlorine emissions were included.

https://doi.org/10.5194/egusphere-2025-23
Preprint. Discussion started: 21 January 2025

On the other hand, numerous studies have emphasized not only the significance of chlorine chemistry but also the influences of the synergistic effects of bromine and iodine chemistry with chlorine chemistry (Sarwar et al., 2019; Simpson et al., 2015; Caram et al., 2023). For instance, modeling studies considering both bromine and iodine chemistries showed that simulated O_3 levels actually decreased by 15.9 ppb (Parrella et al., 2012; Sarwar et al., 2015; Herrmann et al., 2022; Gantt et al., 2017; Read et al., 2008; Huang et al., 2021). These findings strongly suggest that incorporating chlorine processes, together with bromine and iodine processes, is crucial for correct and comprehensive understanding of atmospheric chemistry.

The Korean Peninsula, surrounded by the Yellow Sea, Korea Strait, and the East Sea, is characterized by high population density and highly industrial regions. Therefore, it can be influenced by both natural (oceanic) and anthropogenic halogen emissions. However, almost no modeling study has taken into account the natural and anthropogenic halogen processes over/around South Korea. Although almost no research has been carried out to examines the impacts of halogen chemistry on atmospheric composition over/around South Korea, several studies have considered atmospheric chlorine processes using 3D chemical-transport models (CTMs) (e.g., Jo et al., 2023; Kim et al., 2023). Given the synergistic effects of chlorine, bromine and iodine chemistries in the atmosphere, a comprehensive study that takes all these halogen processes into account is absolutely necessary.

For the comprehensive analysis of halogen processes, we established anthropogenic and natural halogen emissions and incorporated full sets of halogen reactions into the framework of the Community Multi-scale Air Quality (CMAQ) model. The primary objective of this study is to develop improved atmospheric halogen processes with updated (modified) halogen chemistry. We then investigate the formation of ozone using the new halogen processes,

https://doi.org/10.5194/egusphere-2025-23
Preprint. Discussion started: 21 January 2025

also exploring the impacts of the halogen radicals on the mixing ratios of the key atmospheric species such as OH, HO_2, HCHO, VOC_s, and NO_x.

To achieve these research goals, we incorporated the following halogen processes into the CMAQ model: (i) atmospheric chlorine processes (anthropogenic HCl and Cl_2 emissions with 58 chlorine reactions); (ii) atmospheric bromine processes (anthropogenic and natural HBr and Br_2 emissions together with 64 bromine reactions); and (iii) atmospheric iodine processes (HOI and I_2 natural emissions, along with 55 iodine reactions). After these works, we evaluated the performances of the modified CMAQ model against field observations obtained from the Korea US Air Quality (KORUS-AQ) campaign (May – June, 2016).

2. Methodology

In this study, we incorporated homogeneous, aqueous, and heterogeneous halogen reactions into the CMAQ model, along with emissions of halogen species. To evaluate the accuracy of these halogen processes, we compared the model results with observation data from the KORUS-AQ campaign. This section provides several details on the observation data, the WRF-CMAQ model configurations, and the atmospheric halogen processes, including halogen reactions and emissions.

2.1 Observation data

Mixing ratios of nitryl chloride ($ClNO_2$) were measured every five minutes at Olympic Park (37.52°N; 127.12°E) and Mt.Taewha (37.27°N; 127.41°E) stations during the period of the KORUS-AQ campaign (refer to two blue stars in Fig. 1a), using Chemical Ionization Mass Spectrometer (CIMS). The CIMS instrument has a detection limit of 1.5ppt and an uncertainty within 20%. Further details on the CIMS instrument are found in Slusher et al. (2004) and Jeong et al. (2019). In our study, $ClNO_2$ observations were utilized to evaluate the performances of modified CMAQ model simulations. These results are discussed in Sect. 3.1.

https://doi.org/10.5194/egusphere-2025-23
Preprint. Discussion started: 21 January 2025

2.2 WRF-CMAQ model description

The Weather Research and Forecasting (WRF) v3.8.1 model simulations were carried out to generate meteorological fields (Skamarock et al., 2008). The details of physical parameters used in the WRF simulations are summarized in Table S1. National Center for Environmental Prediction Final Analysis (NCEP-FNL) data were used for initial and boundary conditions. The WRF model included a 5-day spin-up period to minimize uncertainties from the initial and boundary conditions.

This study also included the CMAQ v5.2.1 model simulations (Byun and Schere, 2006) over a domain covering northeast Asia with 273 × 204 horizontal grid cells. The grid resolution is 15 × 15 km^2 with 15 vertical layers from surface to 50 hPa. The Statewide Air Pollution Research Center-07 (SAPRC-07TC) mechanism (Carter, 2010; Hutzell et al., 2012) with AERO6 module was used in the CMAQ model simulations. One limitation of the SAPRC-07TC mechanism is that it has only basic chlorine chemistry. In order to implement more sophisticated halogen model simulations, we incorporated additional and updated halogen reactions into the SAPRC-07TC mechanism. The detailed reactions are explained in Sects. 2.4.1 and 2.4.2.

In order to derive the CMAQ model, biomass burning and biogenic emissions were obtained from the Fire Inventory from NCAR (FINN) v1.5 (Wiedinmyer et al., 2011) and the Model of Emissions of Gases and Aerosol from Nature (MEGAN) v2.1 (Guenther et al., 2012), respectively. Anthropogenic emissions were acquired from the KORUS v5.0 emission inventory (Woo et al., 2020), specifically developed for the KORUS-AQ campaign. The KORUS v5.0 inventory covers emissions of primary pollutants such as NO_x, CO, HCHO, VOCs, and particulate chlorine (pCl^-), but it omits the emissions for anthropogenic chlorine species (HCl and Cl_2), bromine species (HBr and Br_2), and ocean-generated halogen species (HOI, I_2, and halocarbons). We have thus developed new halogen emissions for this study. The

https://doi.org/10.5194/egusphere-2025-23
Preprint. Discussion started: 21 January 2025

methodology for developing the halogen emissions will be discussed in Sections 2.3.1 and 2.3.2.

2.3 Halogen emissions

In this section, we discuss the development of anthropogenic and natural halogen emissions within our model framework.

2.3.1 Anthropogenic emissions

First, we assumed that emissions of anthropogenic HCl and Cl_2 are mainly originated from coal combustion. Coal combustion occurs predominantly in four main sectors: industry, residential areas, power plants, and other sectors such as agriculture and furniture manufacturing. In addition, HCl emissions are also taking place from municipal solid waste incineration.

To calculate chlorine emissions from industry and residential areas, we utilized coal consumption data from the 2016 Regional Energy Report of South Korea (https://www.keei.re.kr). Thereafter, the emissions of HCl and Cl_2 from these sectors were calculated using the following equation (1):

$$E_{i,j} = M_{i,j} \times EF_{i,j} \times \rho \times \frac{1}{MM} \times \frac{1}{10^3} \quad \text{(Eq. 1)}$$

where, $E_{i,j}$ represents the emission for species i in categories j (Mg); M denotes the coal consumption (Gg); and EF is the emission factor (μg/g) calculated using the method from a previous study (Jiang et al., 2005 (in Chinese)). ρ indicates the percentage of HCl and Cl_2 in the chlorine content of coal. In our study, percentages of 86.3% and 3.63% for ρ_{HCl} and ρ_{Cl2} were used, respectively, based on research conducted by Deng et al. (2014) and Liu et al. (2018). MM represents the ratios of the molar mass of the chlorine atom to the molecular weight (i.e., 35.5/36.5 for HCl and 1 for Cl_2).

For the remaining three sectors, namely power plants, solid waste incineration, and others, the HCl emissions were obtained directly from the Korean tele-monitoring system

https://doi.org/10.5194/egusphere-2025-23
Preprint. Discussion started: 21 January 2025

(TMS) named the CleanSYS (https://cleansys.or.kr). Meanwhile, the emissions of Cl_2 from these sectors can also be calculated using equation (1), based on the HCl emissions previously calculated.

Bromine emissions (HBr and Br_2) were additionally estimated from the previously calculated chlorine emissions. According to a recent study, bromine is also emitted from the coal combustion with a ratio (0.25) of bromine to chlorine concentrations (Peng and Wu, 2014). These bromine emissions were splitted into 70% and 30% for HBr and Br_2, respectively. The detailed methodology used in our study is summarized in Li et al. (2021).

Consequently, we developed an emission inventory that includes anthropogenic chlorine and bromine emissions. Figure 1 illustrates the spatial distributions of these emissions across South Korea. The total emission rates for anthropogenic HCl, Cl_2, HBr, and Br_2 in South Korea are 5,989.6, 450.8, 460.8, and 240.8 $Mg \cdot yr^{-1}$ respectively. In contrast, Kim et al. (2023) reported smaller emission fluxes for HCl over the same region. These discrepancies may result from the inclusion of additional HCl emissions from the residential and industrial sectors in our study. Moreover, our research also accounts for emissions of Cl_2, HBr and Br_2. It is noteworthy that Cl_2, HBr, and Br_2 have relatively shorter e-folding lifetimes (few minutes for Cl_2 and Br_2, and few hours for HBr) than HCl (about 1.5 days), which may increase the oxidant capacity in the atmosphere.

https://doi.org/10.5194/egusphere-2025-23
Preprint. Discussion started: 21 January 2025

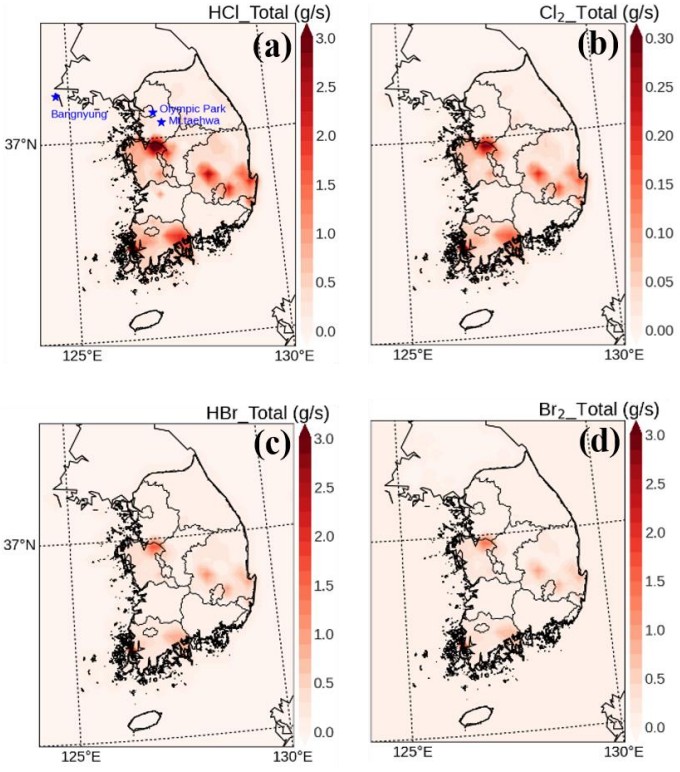

Figure 1. Spatial distributions of anthropogenic emission rates of (a) HCl, (b) Cl_2, (c) HBr, and (d) Br_2 during the period of the KORUS-AQ campaign over South Korea. Three blue stars denote the locations of three supersites (Bangnyung, Olympic Park, and Mt. Taehwa) during the KORUS-AQ campaign.

2.3.2 Natural emissions

Biogenic halocarbons, such as $CHBr_3$, CH_2Br_2, $CHBrCl_2$, CH_2BrCl, $CHBr_2Cl$, CH_2I_2, CH_3I, CH_2ICl, and CH_2IBr, are emitted from micro-algae activities in the ocean. To calculate these emissions of bromine and iodine-containing halocarbon species, we used the chlorophyll-a (chl-a) concentrations as a proxy for the photosynthetic activity of phytoplankton (Liss et al., 2014).

Chlorophyll-a concentrations in ocean have been monitored by various satellite sensors such as Moderate Resolution Imaging Spectroradiometer (MODIS) and Geostationary Ocean Color Imager (GOCI) (Kim et al., 2016; O'reilly and Werdell, 2019; Sarwar et al., 2015).

https://doi.org/10.5194/egusphere-2025-23
Preprint. Discussion started: 21 January 2025

Among these sensors, Park et al. (2015) reported that the chlorophyll-a concentrations measured by the GOCI sensor showed the best agreements with surface observations compared to those from the MODIS sensor in the East Asian ocean. Based on this study, we applied the chlorophyll-a data from the GOCI sensor into our study (refer to Fig. S1).

Gridded halocarbon emissions were estimated using the following equation (2) (Sarwar et al., 2015):

$$E_{Halocarbon} = 1.2 \times 10^{-11} \times (O_F + S_F) \times A_{GC} \times f_{HC} \times f_{DP} \times [chl\text{-}a] \quad \text{(Eq.2)}$$

where, O_F and S_F represent the ocean and coastal fractions of the grid cell, respectively. A_{GC} denotes the area of the grid cell (m^2). f_{HC} is the emission factor for the species; and f_{DP} represents the diurnal profile. [*chl-a*] means the chlorophyll-a concentration.

Natural Br_2 emissions were estimated by debromination of sea-salt aerosols (SSAs), which were derived using the mass ratios of Br to NaCl within SSAs. In addition, inorganic iodine (such as HOI and I_2) emissions were calculated at the air-sea water interfaces, utilizing information on dry deposition of O_3 over the ocean. This approach is based on the fact that the formations of HOI and I_2 are initiated by reaction between iodide (I^-(aq)) and O_3 at the ocean surfaces. Sarwar et al. (2015) employed the same methodology for developing these emissions. The distributions of natural bromine and iodine emissions are shown in Fig. S2.

2.4 Halogen chemical reactions

As mentioned previously, the CMAQ v5.2.1 model considered only simple chlorine reactions. Therefore, we attempted to incorporate the multi-phase halogen reactions into the CMAQ v5.2.1 model to investigate the influences of atmospheric halogen chemistries. Detailed descriptions of these reactions are provided in the subsequent sections.

2.4.1 Chlorine reactions

The chlorine-related reactions were incorporated into the framework of SAPRC07-TC mechanism. The chlorine reactions consist of: (i) adjusted reaction rate coefficients for 14

https://doi.org/10.5194/egusphere-2025-23
Preprint. Discussion started: 21 January 2025

reactions (refer to R9 to R22 in Table 1); (ii) updated 29 gaseous chlorine reactions (refer to R23 to R51 in Table 1); (iii) added two aqueous-phase reactions (refer to R1 to R2 in Table 2); and (iv) incorporated four heterogeneous reactions involving three reactive halogen species, HOCl, $ClNO_2$, and $ClONO_2$, with NO_2 partitioning onto chloride-containing particles (refer to R2 to R6 in Table 3).

The parameterization of γ_{N2O5} currently embedded in the CMAQ v5.2.1 model (shown in R8) has not been greatly satisfactory for reproducing the atmospheric levels of $ClNO_2$.

$$N_2O_5 + (1\text{-}\varphi)H_2O + \varphi Cl^{-1} \xrightarrow{\gamma_{N2O5}} (2\text{-}\varphi)HNO_3 + \varphi ClNO_2 \quad \text{(R8)}$$

where, φ represents the yield of $ClNO_2$ as a function of the concentration of particulate chloride [Cl^-] and aerosol water content [H_2O]. The calculation of φ was proposed by Bertram and Thornton (2009):

$$\varphi = \frac{1}{1+\frac{[H2O]}{483[Cl-]}} \quad \text{(Eq. 3)}$$

Although the use of R8 and Eq. 3 have been an advance in considering the production of $ClNO_2$ from chlorine-containing particles (Bertram and Thornton, 2009), several studies have reported that the parameterizations of γ_{N2O5} with R8 and Eq. 3 tend to produce excessive amounts of nitrate and $ClNO_2$ (Riedel et al., 2012a; Li et al., 2016; Yu et al., 2020). This overestimation may result from uncertainties in calculating aerosol water content ([H_2O]) estimated from the aerosol thermodynamic module (Chang et al., 2016). To deal with this issue, several studies have explored different parameterizations of γ_{N2O5}. However, the γ_{N2O5} still appears to be over-estimated in many cases (e.g., Chang et al., 2016; Liu et al., 2019; Mcduffie et al., 2018; Riedel et al., 2012a; Wang et al., 2017). In this context, we alternatively selected a different parameterization for γ_{N2O5} (see equations (4) to (7)). These parameterizations were suggested by Riemer et al. (2003) and Evans and Jacob (2005):

https://doi.org/10.5194/egusphere-2025-23
Preprint. Discussion started: 21 January 2025

$$\gamma_{N2O5} = f \times \gamma_1 + (1 - f) \times \gamma_2 \quad \text{(Eq. 4)}$$

$$f = \frac{m_{sulfate}}{m_{sulfate} + m_{nitrate}} \quad \text{(Eq. 5)}$$

$$\gamma_1 = \alpha \times 10^{\beta} \quad \text{(Eq. 6)}$$

$$\gamma_2 = 0.1 \times \gamma_1 \quad \text{(Eq. 7)}$$

where α is set to be $2.79 \times 10^{-4} + 1.3 \times 10^{-4} \times RH - 3.43 \times 10^{-4} \times RH^2 + 7.52 \times 10^{-8} \times RH^3$. β is set at 0.48, when $T < 282$ K, or at $4 \times 10^{-2} \times (294 - T)$, when $T \geq 282$ K. m_i represents the aerosol mass concentration of species i. Complete lists of chlorine reactions embedded into the SAPRC07TC mechanism are shown in Tables 1, 2, and 3.

https://doi.org/10.5194/egusphere-2025-23
Preprint. Discussion started: 21 January 2025

Table 1. List of homogeneous chlorine reactions used in this study.

No	Reaction	Reaction rate	Reference
R1	$Cl_2 \xrightarrow{h\nu} 2Cl$	#1.0/<Cl_2>	1
R2	$ClNO \xrightarrow{h\nu} Cl + NO$	#1.0/<ClNO>	1
R3	$Cl + NO_2 + M = ClONO$	1.3e-30^-2.0&1.0e-10^-1.0&-1.0&0.6&1.0	1
R4	$Cl + NO_2 + M = ClNO_2$	1.8e-31^-2.0&1.0e-10^-1.0&-1.0&0.6&1.0	1
R5	$ClONO \xrightarrow{h\nu} Cl + NO_2$	#1.0/<ClONO>	1
R6	$Cl + NO_3 = ClO + NO_2$	2.4×10^{-11}	1
R7	$ClO + NO_2 = ClONO_2$	1.80e-31^-3.4&1.5e-11^-1.90&0.6&1.0	1
R8	$HOCl \xrightarrow{h\nu} Cl + OH$	#1.0/<HOCl>	1
R9	$ClONO_2 = Cl + NO_3$	#1.0/<$ClONO_{2\_1}$>	2
R10	$ClONO_2 = ClO + NO_2$	#1.0/<$ClONO_{2\_2}$>	2
R11	$Cl + NO + M = 2ClNO$	$7.70 \times 10^{-32}(\frac{T}{300})^{-1.8}$	2
R12	$ClNO_2 \xrightarrow{h\nu} Cl + NO_2$	#1.0/<$ClNO_2$>	2
R13	$Cl + HO_2 = HCl$	$1.4 \times 10^{-11}e^{270/T}$	2
R14	$Cl + HO_2 = ClO + OH$	$3.6 \times 10^{-11}e^{-375/T}$	2
R15	$Cl + O_3 = ClO$	$2.3 \times 10^{-11}e^{200/T}$	2
R16	$ClO + NO = Cl + NO_2$	$6.4 \times 10^{-12}e^{290/T}$	2
R17	$ClONO_2 = ClO + NO_2$	2.0×10^{-21}	2
R18	$Cl + ClONO_2 = Cl_2 + NO_3$	$6.5 \times 10^{-12}e^{135/T}$	2
R19	$ClO + HO_2 = HOCl$	$2.6 \times 10^{-12}e^{290/T}$	2
R20	$ClO + ClO = Cl_2 + O_2$	$1.0 \times 10^{-11}e^{-1590/T}$	2
R21	$OH + HCl = Cl$	$1.8 \times 10^{-12}e^{-250/T}$	2
R22	$Cl + H_2 = HCl + HO_2$	$3.1 \times 10^{-11}e^{-2270/T}$	2
R23	$ClO + O = Cl + O_2$	$2.8 \times 10^{-11}e^{85/T}$	2
R24	$ClO + OH = Cl + HO_2$	$7.4 \times 10^{-12}e^{270/T}$	2
R25	$ClO + OH = HCl + O_2$	$6.0 \times 10^{-13}e^{230/T}$	2
R26	$HOCl + OH = ClO + H_2O$	$3.0 \times 10^{-12}e^{-500/T}$	2
R27	$HOCl + O = ClO + OH$	1.7×10^{-13}	2
R28	$ClNO_2 + OH = HOCl + NO_2$	$2.4 \times 10^{-12}e^{-1250/T}$	2
R29	$ClONO_2 + O = ClO + NO_3$	$3.6 \times 10^{-12}e^{-840/T}$	2
R30	$ClONO_2 + OH = HOCl + NO_3$	$1.2\times 10^{-12}e^{-330/T}$	2
R31	$HCl + O = Cl + OH$	$1.0 \times 10^{-11}e^{-3300/T}$	2
R32	$Cl + ClNO = NO + Cl_2$	$5.8 \times 10^{-11}e^{100/T}$	2
R33	$Cl + HOCl = OH + Cl_2$	$3.4 \times 10^{-12}e^{-130/T}$	2
R34	$ClO \xrightarrow{h\nu} Cl + O$	#1.0/<ClO>	2
R35	$Cl + H_2O_2 = HCl + HO_2$	$1.1 \times 10^{-11}e^{-980/T}$	2
R36	$OH + Cl_2 = HOCl + Cl$	$2.6 \times 10^{-12}e^{-1100/T}$	2
R37	$Cl + HNO_3 = HCl + NO_2$	2.0×10^{-16}	2
R38	$Cl_2O_2 \xrightarrow{h\nu} Cl + ClO_2$	#1.0/<Cl_2O_2>	2
R39	$ClO_2 \xrightarrow{h\nu} ClO + O_2$	#1.0/<ClO_2>	2
R40	$Cl + ClO_2 = 2ClO$	1.2×10^{-11}	2
R41	$Cl + ClO_2 = Cl_2 + O_2$	2.3×10^{-10}	2
R42	$OH + Cl_2O_2 = HOCl + ClO_2$	$6.0 \times 10^{-13}e^{670/T}$	2
R43	$OH + ClO_2 = HOCl + O_2$	$1.4\times 10^{-12}e^{600/T}$	2
R44	$Cl_2 + O_2 + M = Cl_2O_2$	2.2e-33^3.1&1.8e-10^0&-1.0&0.6&1.0	2
R45	$ClO + ClO + M = ClO_2$	1.9e-32^3.6&3.7e-12^1.6&-1.0&0.6&1.0	2
R46	$ClO_2 + O = ClO$	$2.4 \times 10^{-12}e^{-960/T}$	2
R47	$NO + ClO_2 = ClO + NO_2$	$6.0 \times 10^{-13}e^{-670/T}$	2
R48	$HCl + NO_3 = HNO_3 + Cl$	5.0×10^{-17}	2
R49	$Cl + Cl_2O_2 = Cl_2 + ClO$	$6.2 \times 10^{-11}e^{130/T}$	2
R50	$ClO + O_3 = ClO_2$	$2.0 \times 10^{-12}e^{-3600/T}$	2
R51	$ClO + NO_3 = ClO_2 + NO_2$	4.7×10^{-13}	2

1. Sander et al. (2010); 2. Burkholder et al. (2020)

https://doi.org/10.5194/egusphere-2025-23
Preprint. Discussion started: 21 January 2025

Table 2. List of aqueous-phase chlorine and bromine reactions used in this study.

No	Species	Reaction	Reaction rate (unit: M/s)	Reference
R1	HOCl	$HOCl + HSO_3^- \xrightarrow{k} SO_4^{2-} + Cl^- + 2H^+$	2.8×10^5	1
R2	HOCl	$HOCl + SO_3^{2-} \xrightarrow{k} SO_4^{2-} + HCl$	7.6×10^8	1
R3	HOBr	$HOBr + HSO_3^- \xrightarrow{k} SO_4^{2-} + HBr$	5.0×10^9	1
R4	HOBr	$HOBr + SO_3^{2-} \xrightarrow{k} SO_4^{2-} + HBr$	2.6×10^7	1

1. Liu and Abbatt. (2020)

Table 3. List of heterogeneous halogen reactions and the uptake coefficients of gases used in this study.

No	Gas	Reaction	Uptake Coefficient (γ_{gas})	Reference
R1	N_2O_5	$N_2O_5 + (1\text{-}\varphi)H_2O + \varphi Cl^- \rightarrow (2\text{-}\varphi) HNO_3 + \varphi ClNO_2$	Function of aerosol mass concentrations, relative humidity, and temperature	1, 2
R2	HOCl	$HOCl + Cl^- = Cl_2$	1.09×10^{-3}	3
R3	$ClONO_2$	$ClONO_2 + Cl^- = Cl_2 + NO_3^-$	0.002	4
R4	$ClNO_2$	$ClNO_2 + Cl^- + H^+ = Cl_2 + HONO$	2.65×10^{-6} (pH < 2.0)	5
R5	$ClNO_2$	$ClNO_2 = Cl^- + NO_3^- + 2H^+$	6×10^{-6} (pH > 2.0)	6
R6	NO_2	$2NO_2 + Cl^- = ClNO + NO_3^-$	10^{-4}	7
R7	HOBr	$HOBr + Br^- = Br_2$	0.08	8
R8	HOBr	$HOBr + Cl^- = BrCl$	0.02	8
R9	$BrONO_2$	$BrONO_2 + H_2O = HOBr + HNO_3$	0.03	9
R10	HBr	$HBr = Br^-$	$1.3 \times 10^{-8} e^{\frac{4290}{T}}$	10
R11	$IONO_2$	$IONO_2 + Cl^- = ICl + HNO_3$	0.005	11
R12	$IONO_2$	$IONO_2 + Br^- = IBr + HNO_3$	0.005	11
R13	INO_2	$INO_2 + Cl^- = ICl + HONO$	0.01	11
R14	INO_2	$INO_2 + Br^- = IBr + HONO$	0.01	11
R15	HOI	$HOI + Cl^- = ICl$	0.005	12
R16	HOI	$HOI + Br^- = IBr$	0.005	12
R17	I_2O_2	$I_2O_2 =$	0.02	12
R18	I_2O_3	$I_2O_3 =$	0.02	12
R19	I_2O_4	$I_2O_4 =$	0.02	12

1. Riemer et al. (2003); 2. Evans and Jacob (2005); 3.Pratte and Rossi (2006); 4.Chen et al. (2022); 5.Riedel et al. (2012); 6.Roberts et al. (2009); 7.Abbatt and Waschewsky (1998); 8.Fernandez et al. (2014); 9.Deiber et al. (2004); 10.Ammann et al. (2013); 11.Saiz Lopez et al. (2014); 12.Sherwen et al. (2016)

https://doi.org/10.5194/egusphere-2025-23
Preprint. Discussion started: 21 January 2025

2.4.2 Bromine reactions

We also incorporated bromine reactions into the SAPRC07-TC mechanisms. The reactions incorporated include: (i) updated absorption cross-sections for BrCl, BrCHO, $CHBr_2Cl$, $CHBr_3$, and $CHBrCl_2$ (refer to R29 to R33 in Table 4); (ii) updated reaction rates for formaldehyde (HCHO) and acetaldehyde (CCHO) reacting with bromine radicals (refer to R34 and R35 in Table 4); (iii) Br-initiated VOC reactions (refer to R36 to R56 in Table 4); (iv) two inter-halogen species reactions (refer to R57 and R58 in Table 4); (v) two aqueous-phase reactions (refer to R3 to R4 in Table 2); and (vi) four heterogeneous reactions for bromine species (refer to R7 to R10 in Table 3). A complete list of the bromine reactions can be found in Tables 2, 3, and 4.

https://doi.org/10.5194/egusphere-2025-23
Preprint. Discussion started: 21 January 2025

Table 4. List of homogeneous bromine reactions used in this study.

No	Reaction	Reaction rate	Reference
R1	$BrO \xrightarrow{h\nu} Br + O^3P$	#1.0/<BrO>	1
R2	$HOBr \xrightarrow{h\nu} Br + OH$	#1.0/<HOBr>	1
R3	$BrNO_3 \xrightarrow{h\nu} Br + NO_3$	#1.0/<$BrNO_3$_1>	1
R4	$BrNO_3 \xrightarrow{h\nu} BrO + NO_2$	#1.0/<$BrNO_3$_2>	1
R5	$BrNO_2 \xrightarrow{h\nu} Br + NO_2$	#1.0/<$BrNO_2$>	1
R6	$Br_2 \xrightarrow{h\nu} 2Br$	#1.0/<Br_2>	1
R7	$Br + O_3 = BrO$	$1.6 \times 10^{-11}e^{-780/T}$	1
R8	$BrO + HO_2 = HOBr$	$4.5 \times 10^{-12}e^{460/T}$	1
R9	$Br + HO_2 = HBr$	$4.8 \times 10^{-12}e^{-310/T}$	1
R10	HBr + OH = Br	$6.7 \times 10^{-12}e^{155/T}$	1
R11	BrO + BrO = 2Br	$1.4 \times 10^{-12}e^{210/T}$	1
R12	BrO + BrO = Br_2	$2.9 \times 10^{-14}e^{840/T}$	1
R13	BrO + NO = Br + NO_2	$8.8 \times 10^{-12}e^{260/T}$	1
R14	$Br + BrNO_3 = Br_2 + NO_3$	4.9×10^{-11}	1
R15	Br_2 + OH = HOBr + Br	$2.1 \times 10^{-11}e^{240/T}$	1
R16	BrO + OH = Br + HO_2	$1.7\times 10^{-11}e^{250/T}$	1
R17	$Br + NO_3 = BrO + NO_2$	1.6×10^{-11}	1
R18	BrO + ClO = Br + Cl	$4.7 \times 10^{-12}e^{320/T}$	1
R19	BrO + MEO2 = 0.8HOBR + 0.2BR + 0.3HCOOH + 0.2HCHO + 0.13OH + 0.13HO_2	$2.65 \times 10^{-14}e^{1600/T}$	1
R20	CH3Br + OH = Br	$1.42 \times 10^{-12}e^{-1150/T}$	1
R21	$MB3^a$ + OH = 3Br	$9.0 \times 10^{-13}e^{-360/T}$	1
R22	$MB2^b$ + OH = 2Br + HO_2	$2.0 \times 10^{-12}e^{-840/T}$	1
R23	$MB2C^c$+ OH = 2Br + Cl	$9.0\times 10^{-13}e^{-420/T}$	1
R24	$MBC2^d$ + OH = Br + 2Cl	$9.4 \times 10^{-13}e^{-510/T}$	1
R25	$MBC2^e$ + OH = Br + Cl + HO_2	$2.1 \times 10^{-12}e^{-880/T}$	1
R26	DMS + BrO = 0.75SO_2 + 0.25MSA +MEO2 + Br	$1.5 \times 10^{-14}e^{1000/T}$	1
R27	BrO + NO_2 = $BrNO_3$	5.2e-31^3.2&6.9e-12^-2.9&0.6&1.0	1
R28	Br + NO_2 = $BrNO_2$	4.2e-31^2.4&2.7e-11^0.0&0.6&1.0	1
R29	$BrCl \xrightarrow{h\nu} Br + Cl$	#1.0/<BrCl>	2
R30	$FMBR^f \xrightarrow{h\nu} Br + CO + HO2$	#1.0/<FMBR>	2
R31	$MB3^a \xrightarrow{h\nu} 3.0Br + HO_2$	#1.0/<MB3>	2
R32	$MB2C^c \xrightarrow{h\nu} 2.0Br + Cl + HO_2$	#1.0/<MB2C>	2
R33	$MBC2^d \xrightarrow{h\nu} Br + 2.0Cl + HO_2$	#1.0/<MBC2>	2
R34	HCHO + Br = HBr + HO_2	$7.7 \times 10^{-12}e^{-580/T}$	2
R35	CCHO + Br = HBr + $MECO_3$	$1.8 \times 10^{-11}e^{-460/T}$	2
R36	ETHE + Br = $FMBR^f$ + HCHO + HO2 + RO2C	1.3×10^{-13}	2
R37	OLE1 + Br = $FMBR^f$ + CCHO + HO2 + RO2C	3.6×10^{-12}	2
R38	OLE2 + Br = $FMBR^f$ + 0.75RCHO + 0.15ACET +0.1MEK + HO2 + RO2C	1.0×10^{-11}	2
R39	ISOPRENE + Br = $FMBR^f$ + PRD2 + HO2 + RO2C	7.5×10^{-11}	2
R40	$FMBR^f$ + OH = Br + CO	5.0×10^{-12}	2
R41	RCHO + Br = HBr + RCO3	$1.8 \times 10^{-11}e^{-460/T}$	2
R42	GLY + Br = HBr + 2CO + HO2	$7.7 \times 10^{-12}e^{-580/T}$	2
R43	MGLY + Br = HBr + CO + MECO3	$1.8 \times 10^{-11}e^{-460/T}$	2
R44	BALD + Br = HBr + BZCO3	$1.8 \times 10^{-11}e^{-460/T}$	2
R45	ACROLEIN + Br = 0.75 $FMBR^f$ + 0.25HBr + 0.25MACO3 + 0.75MGLY + 0.75HO2	1.0×10^{-11}	2
R46	Benzene + Br = Product	1.0×10^{-11}	3
R47	Toluene + Br = Product	1.0×10^{-14}	4
R48	o-xylene + Br = Product	1.6×10^{-14}	4
R49	m-xylene + Br = Product	7.9×10^{-14}	4
R50	p-xylene + Br = Product	4.0×10^{-14}	4
R51	α-pinene + Br = Product	6.8×10^{-14}	5
R52	MACR + Br = Product	3.9×10^{-10}	5
R53	MVK + Br = Product	2.3×10^{-10}	5
R54	MEK + Br = Product	3.6×10^{-10}	5
R55	ETOH + Br = Product	$8.6 \times 10^{-11}e^{45/T}$	5
R56	MEOH +Br = Product	5.5×10^{-11}	5
R57	Cl + BrCl = Br + Cl_2	1.45×10^{-11}	6
R58	Cl + Br_2 = BrCl + Br	1.94×10^{-10}	7

1. Sherwen et al. (2016); 2. Burkholder et al. (2020); 3. Keefer et al. (1950); 4. Giri et al. (2022); 5. Qinyi et al. (2021); 6. Clyne and Cruse. (1972); 7.Khamaganov and Crowley. (2010)

$MB3^a$ = $CHBr_3$, $MB2^b$ = CH_2Br_2, $MB2C^c$ = CH_2Br_2, $MBC2^d$ = $CHBr_2Cl$, MBC^e = CH_2ClBr, $FMBR^f$ = BrCHO

https://doi.org/10.5194/egusphere-2025-23
Preprint. Discussion started: 21 January 2025

2.4.3 Iodine reactions

Iodine reactions taken into account in this study were acquired from Saiz-Lopez et al. (2014) and Sherwen et al. (2016). We updated iodine reactions in three ways: (i) updated absorption cross-sections for ICl and IBr (refer to R43 and R44 in Table 5); (ii) two inter-halogen species reactions (refer to R45 and R46 in Table 5); and (iii) nine heterogeneous reactions for $IONO_2$, INO_2, HOI, I_2O_2, I_2O_3, and I_2O_4 (refer to R11 to R19 in Table 3). These iodine reactions are shown in Tables 3 and 5.

https://doi.org/10.5194/egusphere-2025-23
Preprint. Discussion started: 21 January 2025

Table 5. List of homogeneous iodine reactions used in this study.

No	Reaction	Reaction rate	Reference
R1	$I_2 \xrightarrow{hv} 2I$	#1.0/<I_2>	1
R2	$HOI \xrightarrow{hv} I + OH$	#1.0/<HOI>	1
R3	$IO \xrightarrow{hv} I + O^3P$	#1.0/<IO>	1
R4	$OIO \xrightarrow{hv} I$	#1.0/<OIO>	1
R5	$INO \xrightarrow{hv} I + NO$	#1.0/<INO>	1
R6	$INO_2 \xrightarrow{hv} I + NO_2$	#1.0/<INO_2>	1
R7	$IONO_2 \xrightarrow{hv} I + NO_3$	#1.0/<$IONO_2$>	1
R8	$I_2O_2 \xrightarrow{hv} I + OIO$	#1.0/<$IONO_2$>	1
R9	$I_2O_3 \xrightarrow{hv} IO + OIO$	#1.0/<$IONO_2$>	1
R10	$I_2O_4 \xrightarrow{hv} 2OIO$	#1.0/<$IONO_2$>	1
R11	$CH_3I \xrightarrow{hv} I + MEO2$	#1.0/<CH_3I>	1
R12	$MIC \xrightarrow{hv} I + Cl$	#1.0/<MIC>	1
R13	$MIB \xrightarrow{hv} I + Br$	#1.0/<INO_2>	1
R14	$MI2 \xrightarrow{hv} 2I$	#1.0/<$IONO_2$>	1
R15	$I + O_3 = IO$	$2.1 \times 10^{-11} e^{-830/T}$	2
R16	$I + HO_2 = HI$	$1.5 \times 10^{-11} e^{-1090/T}$	2
R17	I_2 + OH = HOI + I	2.1×10^{-10}	2
R18	HI + OH = I	$1.6 \times 10^{-11} e^{440/T}$	2
R19	HOI + OH = IO	5.0×10^{-12}	2
R20	$IO + HO_2 = HOI$	$1.4 \times 10^{-11} e^{540/T}$	2
R21	IO + NO = $I + NO_2$	$7.15 \times 10^{-12} e^{300/T}$	2
R22	INO + INO = I_2 + 2NO	$8.4 \times 10^{-11} e^{-2620/T}$	2
R23	$INO_2 + INO_2 = I_2 + NO_2$	$4.7 \times 10^{-13} e^{-1670/T}$	2
R24	$I_2 + NO_3$ = I + $IONO_2$	1.5×10^{-12}	2
R25	$IONO_2$ + I = $I_2 + NO_3$	$9.1 \times 10^{-11} e^{-146/T}$	2
R26	I + BrO = IO + Br	1.2×10^{-11}	2
R27	IO + Br = I + BrO	2.7×10^{-11}	2
R28	IO + BrO = Br + I	$1.5 \times 10^{-11} e^{510/T}$	2
R29	IO + ClO = I + Cl	$4.7 \times 10^{-12} e^{280/T}$	2
R30	OIO + OIO = I_2O_4	1.5×10^{-10}	2
R31	OIO + NO = IO + NO_2	$1.1 \times 10^{-12} e^{542/T}$	2
R32	IO + IO = 0.4OIO + 0.4I + 0.6I_2O_2	$5.4 \times 10^{-11} e^{180/T}$	2
R33	IO + OIO = I_2O_3	1.5×10^{-10}	2
R34	I_2O_2 = OIO + I	$2.5 \times 10^{-14} e^{-9770/T}$	2
R35	I_2O_4 = 2OIO	3.8×10^{-2}	2
R36	$INO_2 = NO_2 + I$	$9.9 \times 10^{17} e^{-11859/T}$	2
R37	$IONO_2 = NO_2$ + IO	$2.1 \times 10^{15} e^{-13670/T}$	2
R38	CH_3I + OH = HCHO	$4.3 \times 10^{-12} e^{-1120/T}$	2
R39	IO + DMS = 0.75SO_2 + 0.25MSA +MEO2	$3.3 \times 10^{-13} e^{-925/T}$	2
R40	I + NO = INO	1.8e-32^-1.0&1.7e-11^0.0&0.6&1.0	2
R41	$I + NO_2 = INO_2$	3.0e-31^-1.0&6.6e-11^0.0&0.6&1.0	2
R42	$IO + NO_2 = IONO_2$	7.7e-31^-3.5&7.7e-12^-.1.5&0.6&1.0	2
R43	$ICl \xrightarrow{hv} I + Cl$	#1.0/<ICl>	3
R44	$IBr \xrightarrow{hv} I + Br$	#1.0/<IBr>	3
R45	$Cl + I_2$ = ICl + I	2.81×10^{-10}	4
R46	$Br + I_2$ = IBr + I	1.2×10^{-10}	5

1. Sherwen et al. (2016); 2. Saiz-Lopez et al. (2014); 3. Burkholder et al. (2020); 4. Baklanov et al. (1997); 5.Bedjanian et al. (1997)

https://doi.org/10.5194/egusphere-2025-23
Preprint. Discussion started: 21 January 2025

2.5 Experimental design

To better understand the impacts of atmospheric halogen chemistries, we designed four experiments: (i) experiment without halogen chemistry (referred to as CTRL); (ii) original CMAQv5.2.1 model simulation only with chlorine processes (EXP_{Cl}); (iii) experiment with both chlorine and bromine processes (EXP_{Cl_Br}); and (iv) experiment with full halogen processes ($EXP_{Cl\_Br\_I}$). The design of these four experiments is explained in Table 6.

In addition, in order to further analyze our results, we carried out two more experiments: (i) CMAQ model runs with the halogen chemistry constructed by Saiz-Lopez et al. (2014) (labeled as EXP_{CAM}); and (ii) CMAQ model run with the halogen chemistry constructed by Sarwar et al. (2015) (labelled as EXP_{CMAQ}). The former halogen chemistry was included in a global CTM named CAM-Chem, while the latter was in the CMAQ model. That is why we labeled these two experiments, EXP_{CAM} and EXP_{CMAQ}, respectively.

Table 6. Description of the four experiments conducted in this study.

Experiment	Chlorine		Bromine		Iodine	
	Emission	Reaction	Emission	Reaction	Emission	Reaction
CTRL	-	-	-	-	-	-
EXP_{Cl}	√	√	-	-	-	-
EXP_{Cl_Br}	√	√	√	√	-	-
$EXP_{Cl\_Br\_I}$	√	√	√	√	√	√

3. Results & Discussions

In this section, we discuss the accuracy of new halogen chemistries and processes through the comparison between simulated and measured mixing ratios of halogen-containing compounds during the period of KORUS-AQ campaign. We then analyze the experimental

https://doi.org/10.5194/egusphere-2025-23
Preprint. Discussion started: 21 January 2025

results to evaluate the impacts of atmospheric halogen chemistries and processes on key-species concentrations in the atmosphere.

3.1 Model performances

3.1.1 Observed vs Modeled $ClNO_2$ mixing ratios

To evaluate the model performances, we used the mixing ratios of $ClNO_2$ observed at two supersites (Olympic Park and Mt. Taehwa stations) in South Korea. Although the mixing ratios of atmospheric Cl_2 were also measured at these two stations, we focused solely on $ClNO_2$ observations due to several uncertainties associated with Cl_2 analysis. These issues will be discussed later in Sect. 3.1.3.

Figure 2 presents the diurnal variations of modeled and observed mixing ratios of $ClNO_2$ at two monitoring stations. The CTRL simulation (black circles and lines in Fig. 2) and EXP_{CAM} (purple circles and lines in Fig. 2) could not reproduce the observed mixing ratios of $ClNO_2$ at the two supersites. For instance, the average mixing ratios of $ClNO_2$ at both monitoring stations were 0.00 ppt for CTRL and 15.40 ppt for EXP_{CAM}, while observed average mixing ratio of $ClNO_2$ was 122.67 ppt. The reason for these large differences may be attributed to uncertainties in the consideration of heterogeneous partitioning of N_2O_5 onto chloride-containing particles in the model (recall R8: $N_2O_5 + (1\text{-}\varphi)H_2O + \eta Cl^- \rightarrow (2\text{-}\varphi)HNO_3 + \varphi ClNO_2$). On the other hand, the EXP_{CMAQ} (blue circles and lines in Fig. 2) and $EXP_{Cl\_Br\_I}$ (red circles and lines in Fig. 2), which accounted for halogen chemistries, tend to better capture the diurnal patterns of observed mixing ratios of $ClNO_2$ (refer to open circles and lines in Fig. 2). These models also demonstrated significant improvements, in terms of statistical metrics (which will be presented in Table 7).

Although the EXP_{CMAQ} showed reasonable agreement, it also exhibited significant biases during the nighttime. Conversely, the $EXP_{Cl\_Br\_I}$ simulation achieved better agreements with the observed mixing ratios of $ClNO_2$ at both stations. For example, the index of

https://doi.org/10.5194/egusphere-2025-23
Preprint. Discussion started: 21 January 2025

agreement (IOA) increased from 0.62 for EXP_{CMAQ} to 0.66 for $EXP_{Cl\_Br\_I}$ and from 0.57 to 0.59 at Olympic Park and Mt.Taehwa stations, respectively. These enhancements suggest that successful implementation of the models depends on not only considering chlorine reactions but also incorporating more comprehensive halogen reactions, as demonstrated by $EXP_{Cl\_Br\_I}$. The following sections will explore and discuss these halogen reactions in the atmosphere.

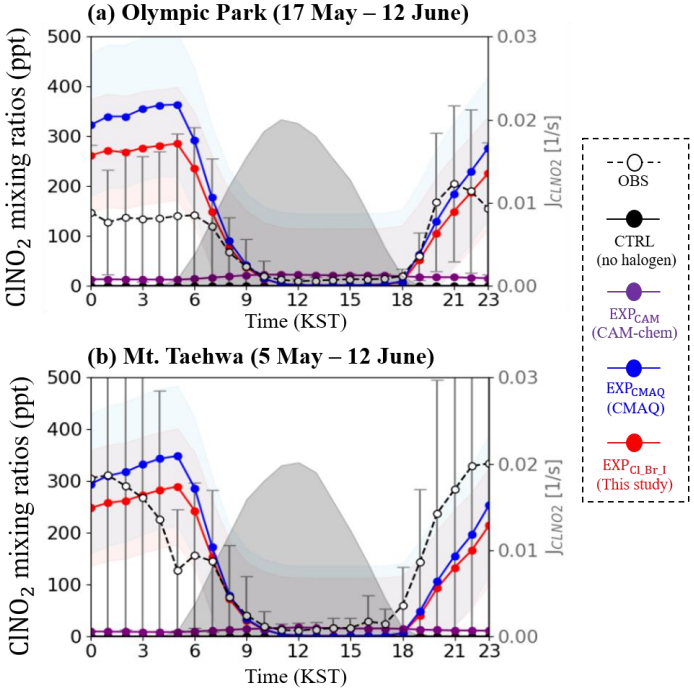

Figure 2. Diurnal variations in the mixing ratios of $ClNO_2$ (unit: ppt) at (a) Olympic Park and (b) Mt.Taehwa stations during the period of the KORUS-AQ campaign. Observed values are represented by open circles (error bars indicate the standard deviation). Colored lines with shaded areas show the hourly-averaged mixing ratios of $ClNO_2$ and the corresponding standard deviation from each simulation. The black shaded area indicates the variations in the photolysis rate of $ClNO_2$ derived from the $EXP_{Cl\_Br\_I}$ simulation.

https://doi.org/10.5194/egusphere-2025-23
Preprint. Discussion started: 21 January 2025

Table 7. Statistical metrics for $ClNO_2$ analysis from CTRL, EXP_{CAM}, EXP_{CMAQ}, and $EXP_{Cl\_Br\_I}$ simulations at the Olympic Park and Mt.Taewha stations during the period of KORUS-AQ campaign.

Target: $ClNO_2$		Olympic Park	Mt.Taehwa
	Observed mean (ppt)	85.97	159.36
CTRL	Modeled mean (ppt)	0	0
	MB (ppt)	-85.97	-159.36
	RMSE (ppt)	150.30	288.82
	IOA	0.41	0.40
EXP_{CAM}	Modeled mean (ppt)	17.31	13.49
	MB (ppt)	-68.67	-145.87
	RMSE (ppt)	143.23	281.78
	IOA	0.37	0.40
EXP_{CMAQ}	Modeled mean (ppt)	135.77	152.89
	MB (ppt)	49.80	-6.65
	RMSE (ppt)	204.42	289.19
	IOA	0.62	0.57
$EXP_{Cl\_Br\_I}$	Modeled mean (ppt)	116.76	134.29
	MB (ppt)	30.79	-25.07
	RMSE (ppt)	174.41	272.69
	IOA	0.66	0.59

3.1.2 Contributions to mixing ratios of $ClNO_2$

Figure 3a and 3c represent the diurnal variations in the mixing ratios of $ClNO_2$ from the EXP_{CMAQ} (blue dotted line) and $EXP_{Cl\_Br\_I}$ simulations (red dotted line) at two supersites during the period of the KORUS-AQ campaign. Through a sensitivity test, we attempted to identify the key reactions in the $EXP_{Cl\_Br\_I}$ causing differences from the EXP_{CMAQ} simulation. From the studies, we identified four critical halogen reactions: (i) updated reaction rate coefficient of R20 in Table 1; (ii) newly-added heterogeneous reaction of HOBr as shown in R8 of Table 3; (iii) modified parameterization of γ_{N2O5} as shown in R1 of Table 3; and (iv) newly-added heterogeneous reaction of NO_2 onto atmospheric aerosols as shown in R6 of Table 3. The contributions of these four reactions were calculated and are presented in blue-, green-, yellow-, and red-shaded areas in Fig. 3, respectively. It appears that the contribution of the parameterization of γ_{N2O5} is the most significant. A detailed analysis of these differences between EXP_{CMAQ} and the $EXP_{Cl\_Br\_I}$ is further discussed in Table S2.

https://doi.org/10.5194/egusphere-2025-23
Preprint. Discussion started: 21 January 2025

Figure 3b and 3d illustrate the contributions of the four reactions to the mixing ratios of $ClNO_2$ at the two supersites. Our result again indicates that selecting the new γ_{N2O5} led to the largest decreases in the averaged mixing ratios of $ClNO_2$ by 9.58 ppt (50.4%) and 7.50 ppt (40.3%) at the Olympic Park and Mt.Taehwa stations, respectively. These reductions are obviously attributed to lower values of γ_{N2O5} in $EXP_{Cl\_Br\_I}$ (γ_{N2O5} = ~0.013), compared to those in EXP_{CMAQ} (γ_{N2O5} = ~0.014) as shown in Fig. S3. Such a small difference in γ_{N2O5} led to substantial differences in the mixing ratios of $ClNO_2$. In addition, the inclusion of reaction (R20) with a reaction rate coefficient reduced by a factor of 10, contributed to the reduction in the mixing ratios of $ClNO_2$ by 3.40 ppt (17.9%) at the Olympic Park station. Accounting for the heterogeneous reaction of NO_2 and HOBr onto chlorine-containing particles also resulted in reductions in the mixing ratios of $ClNO_2$ by 4.46 ppt (24.0%) and 2.77 ppt (14.9%) at the Mt. Taehwa station, respectively.

Collectively, the four reactions mentioned above may be the key reactions that can significantly change the atmospheric levels of $ClNO_2$. Nevertheless, it should also be noted that the $EXP_{Cl\_Br\_I}$ simulation still exhibited discrepancies with the observed mixing ratios of $ClNO_2$. Further studies should investigate the factors causing these discrepancies (such as yield of $ClNO_2$ (φ_{ClNO2}), unknown chlorine emissions, and missing halogen reactions) to enhance our understanding of atmospheric halogen chemistry.

https://doi.org/10.5194/egusphere-2025-23
Preprint. Discussion started: 21 January 2025

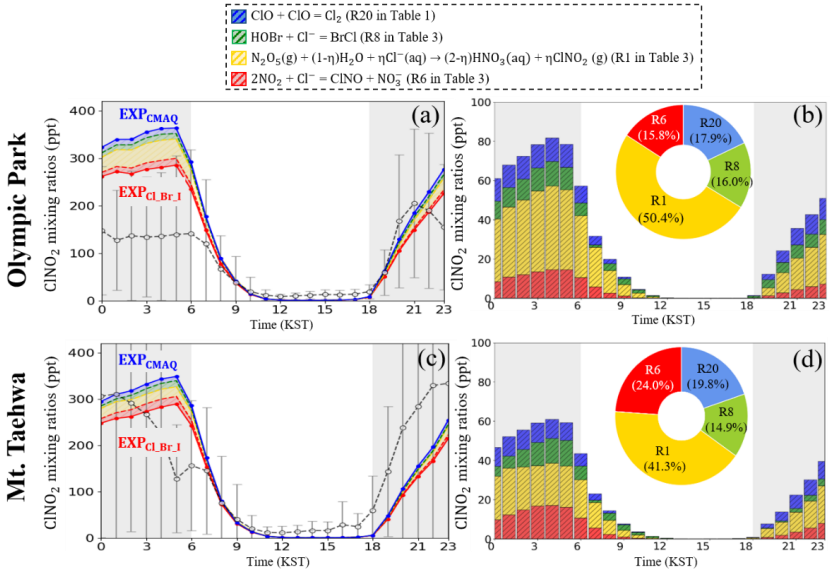

Figure 3. Contributions of halogen reactions to the mixing ratios of $ClNO_2$ in the EXP_{CMAQ} and $EXP_{Cl\_Br\_I}$ simulations at (a and b) Olympic Park and (c and d) Mt. Taehwa stations during the period of KORUS-AQ campaign. Stacked bars and pie charts show the contributions from four halogen reactions to the mixing ratios of $ClNO_2$.

3.1.3 Uncertainties in Cl_2

Figure 4 represents bar graphs of average Cl_2 mixing ratios from the four experiments, together with the observed Cl_2 mixing ratios at two supersites. Among them, the mixing ratios of Cl_2 from the $EXP_{Cl\_Br\_I}$ agree well with the observed mixing ratios of Cl_2. Based on these findings, we attempted to analyze which reactions contributed to elevated levels of Cl_2. Two key reactions were identified: (i) $HOCl + Cl^- \rightarrow Cl_2$ (R2 in Table 3) and (ii) $ClONO_2 + Cl^- \rightarrow Cl_2$ (R3 in Table 3). These reactions accounted for Cl_2 increase of 0.18 ppt (14.2%) and 1.06 ppt (84.1%), respectively, at the two supersites.

Although the current modeling system has improved the predictions of 'campaign-averaged' Cl_2 mixing ratios, it has a serious limitation in reproducing daytime Cl_2 levels, likely due to the extremely fast photo-dissociation rate of Cl_2 (J_{Cl2} is estimated at 2.5×10^{-3} s^{-1}). In

https://doi.org/10.5194/egusphere-2025-23
Preprint. Discussion started: 21 January 2025

other words, once Cl_2 was produced via daytime halogen reaction pathways (see R3 to R5 in Table 3), it is rapidly removed by the fast photo-dissociation. To address this challenge, several studies suggested potential missing daytime reactions, such as particulate nitrate photolysis and the uptake of O_3 and OH onto atmospheric particles (Peng et al., 2022; Chen et al., 2022). However, these reactions also have limitations in perfectly explaining the relatively high levels of Cl_2 during the daytime. The accuracy of simulating daytime Cl_2 mixing ratios remains a topic of further discussion.

In addition, significant uncertainties have been reported in observing Cl_2 mixing ratios using the CIMS instrument. The detection limit for Cl_2 in the CIMS instrument was estimated to be 2.9 ppt over a 30-minute interval (Jeong et al., 2019). However, the averaged mixing ratios of Cl_2 of 2.08 ppt and 2.69 ppt were measured at Olympic Park and Mt. Taehwa, respectively, as depicted in Fig.4. Given that the observed levels of Cl_2 at the two monitoring stations were very close to the detection limit of the instrument, significant uncertainties likely exist in these measurements of the mixing ratios of Cl_2.

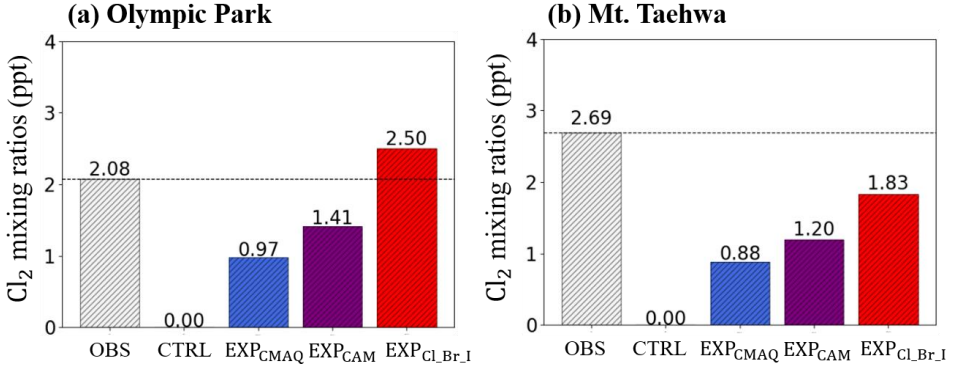

Figure 4. Comparisons of averaged mixing ratios of Cl_2 observed (OBS) and modeled from four simulations (CTRL, EXP_{CMAQ}, EXP_{CAM}, and $EXP_{Cl\_Br\_I}$) at (a) Olympic Park and (b) Mt. Taehwa stations. Dotted lines represent the observed mixing ratios of Cl_2.

https://doi.org/10.5194/egusphere-2025-23
Preprint. Discussion started: 21 January 2025

3.2 Influences of halogen chemistry on O_3 mixing ratios

3.2.1 Comparative analysis at three supersites

Based on the evaluation of model performances, we analyzed the impacts of halogen processes on atmospheric O_3 mixing ratios at three monitoring stations (regarding the locations, see Fig. 1a). Fig. 5 represents the diurnal variations in the mixing ratios of O_3 as simulated from both the CTRL (black circles) and $EXP_{Cl\_Br\_I}$ (red circles), together with the observations (white open circles) during the period of the KORUS-AQ campaign. It shows that the O_3 mixing ratios simulated from the $EXP_{Cl\_Br\_I}$ slightly increased by ~0.06 ppb (0.3%) and ~0.14 ppb (0.4%), higher than those from the CTRL at Olympic Park and Mt. Taehwa stations, respectively. Similar patterns were also observed in the comparisons between O_3 observations from 320 AIR-KOREA stations and O_3 predictions (as shown in Fig. S4).

It should be noted that the simulated O_3 mixing ratios decreased slightly by ~0.19 ppb (0.3%), lower than those simulated from the CTRL at the Bangnyung station. These results raised two questions: (i) why did the opposite patterns take place between two land stations and one ocean station (Bangnyung Island station)? and (ii) what mechanism caused these opposite patterns in the mixing ratios of O_3? To answer these two questions, we further investigated the role of halogen chemistry in atmospheric O_3 chemistry.

https://doi.org/10.5194/egusphere-2025-23
Preprint. Discussion started: 21 January 2025

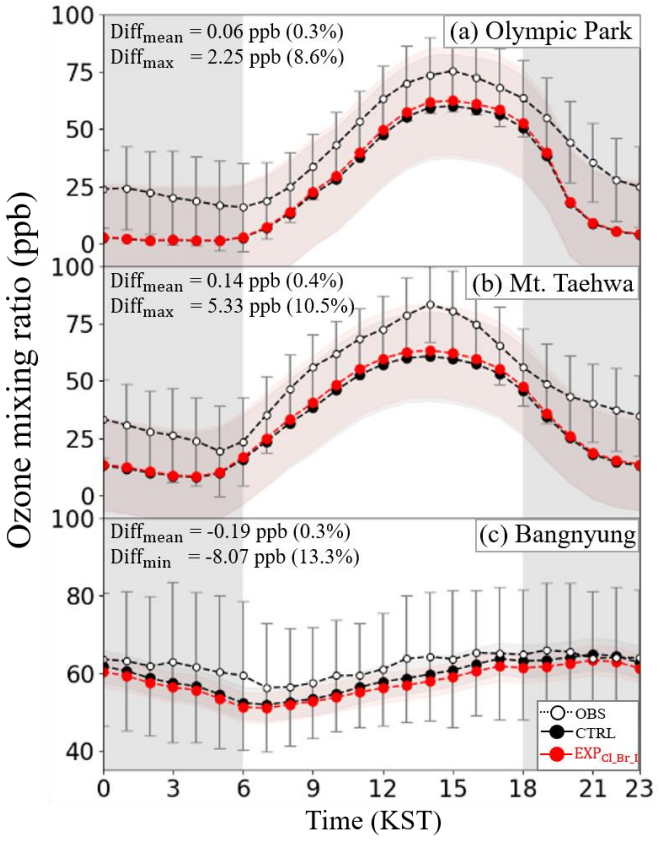

Figure 5. Diurnal variations in the mixing ratios of O_3 from CTRL (black circles) and $EXP_{CL\_Br\_I}$ (red circles) simulations, together with observed mixing ratios of O_3 (OBS; white circles) at (a) Olympic Park, (b) Mt. Taehwa, and (c) Bangnyung stations during the period of the KORUS-AQ campaign. Error bars and grey-shaed areas represent one standard deviations and nighttime, respectively.

3.2.2 Impacts of halogen processes

Figure 6 illustrates the spatial distributions of the differences between two O_3 mixing ratios simulated under the consideration of individual halogen chemistries over the Korean peninsula. The CMAQ-simulated O_3 mixing ratios for EXP_{Cl} showed an increase of 0.62 ppb (1.4%) compared to those from the CTRL over the Korean peninsula (as shown in Fig. 6a).

https://doi.org/10.5194/egusphere-2025-23
Preprint. Discussion started: 21 January 2025

This increase is attributed to the VOC oxidation by Cl radicals, which leads to the production of additional RO_2 radicals. Additional O_3 is subsequently produced via RO_2 + NO reactions. It is well-known that VOC oxidation rates by Cl radicals are approximately 10 times faster than those by OH radicals (Edwards and Young, 2024). Several previous studies have also confirmed these findings (Kim et al., 2023; Jo et al., 2023).

Bromine-containing species are known to contribute to O_3 destruction in the atmosphere. However, VOC oxidations by Br radicals also contribute to atmospheric O_3 formation via the reactions of Br +VOC → product + RO_2 (these reactions are shown in R36 to R57 in Table 4). As a result, the net effects of bromine processes (i.e., $EXP_{Cl\_Br} - EXP_{Cl}$) slightly increase O_3 mixing ratios by ~0.01 ppb, as shown in Fig. 6b. These negligible effects are likely because the decrease in O_3 mixing ratios is almost offset by an increase in O_3 mixing ratios.

In Fig. 6c, when iodine processes were incorporated into the modeling system, the surface-averaged O_3 mixing ratios decreased by ~1.39 ppb (2.4%), particularly over ocean areas. The iodine radicals generated from the photolysis of marine-originated iodine species primarily react with O_3. Given the low levels of VOCs over ocean areas, iodine radicals predominantly participate in the O_3 destruction over the ocean.

Again, the O_3 mixing ratios are controlled by competition between the O_3 production and O_3 destruction. We found that the average O_3 mixing ratios increased by 0.21 ppb (~0.5%) over land areas and decreased by 0.69 ppb (~1.2%) over ocean areas under the considerations of entire halogen processes (i.e., $EXP_{Cl\_Br\_I}$ – CTRL) (refer to Figs. 6d and S5). These findings are closely in line with the increases in O_3 mixing ratios at the Olympic Park and Mt. Taehwa stations (located on land areas) and the decreases in O_3 mixing ratios at the Bangnyung station (located around ocean areas) under the comprehensive considerations of the halogen chemistries, as discussed in Sect. 3.2.1.

https://doi.org/10.5194/egusphere-2025-23
Preprint. Discussion started: 21 January 2025

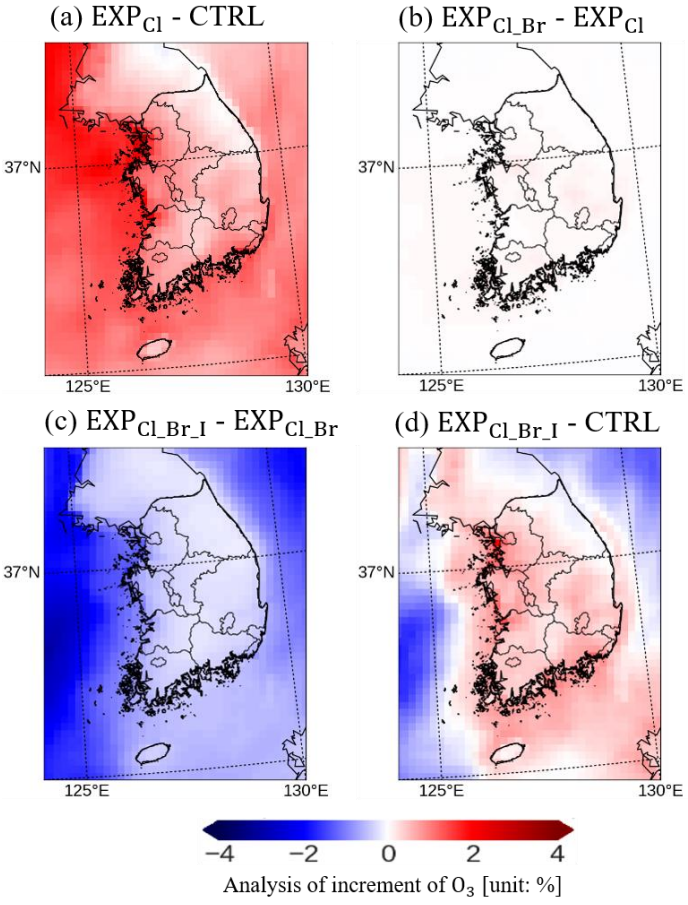

Figure 6. Spatial impacts of (a) chlorine processes (EXP_{Cl} - CTRL), (b) bromine processes (EXP_{Cl_Br} – EXP_{Cl}), (c) iodine processes ($EXP_{Cl\_Br\_I}$ – EXP_{Cl_Br}), and (d) total halogen processes ($EXP_{Cl\_Br\_I}$ – CTRL) on O_3 mixing ratios over the Korean peninsula.

3.2.3 Net O_x production

To better understand the influences of the halogen chemistries on atmospheric O_3 mixing ratios, we additionally carried out a quantitative analysis. We calculated O_x production rates ($P(O_x)$) utilizing a definition of expanded O_x family ($\equiv O_3 + O^{1D} + O^{3p} + NO_2 + 2NO_3 + 3N_2O_5 + XNO_2 + XO + XONO_2$; here, X denotes Cl, Br, and I). The constructions of the $P(O_x)$ are shown in equations (8) to (10):

https://doi.org/10.5194/egusphere-2025-23
Preprint. Discussion started: 21 January 2025

$$F(O_x) = k_{HO_2+NO}[HO_2][NO] + k_{RO_2+NO}[RO_2][NO] \quad \text{(Eq. 8)}$$

$$D(O_x) = k_{NO_2+OH}[NO_2][OH] + k_{O_3+VOC}[O_3][VOC] + k_{O(1D)+H_2O}[O(^1D)][H_2O] + k_{O_3+OH}[O_3][OH] + k_{O_3+HO_2}[O_3][HO_2] + k_{RO_2+NO_2}[RO_2][NO_2] + (k_{ClO+O_3}[O_3] + k_{ClO+NO_2}[NO_2] + k_{ClO+O(3p)}[O(^3P)])[ClO] + k_{Cl+O_3}[Cl][O_3] + k_{BrO+OH}[BrO][OH] + k_{XO+HO_2}[XO][HO_2] + k_{XO+XO}[XO]^2 + k_{NO_3+VOC}[NO_3][VOC] + 3k_{het}[N_2O_5] \quad \text{(Eq. 9)}$$

$$P(O_x) = F(O_x) - D(O_x) \quad \text{(Eq. 10)}$$

where, $F(O_x)$ and $D(O_x)$ represent the O_x formation rates and O_x destruction rates, respectively. k_i and k_{het} denote the reaction rate constants for reaction i and heterogeneous reactions of N_2O_5, respectively.

Figure 7 shows the average O_x formation rates ($F(O_x)$), O_x destruction rates ($D(O_x)$), and the $P(O_x)$ from the CTRL and $EXP_{Cl\_Br\_I}$ simulations. Over land, rates for reactions of RO_2 + NO and HO_2 + NO in the $F(O_x)$ increased from 2.16 ppb/h to 2.21 ppb/h and from 2.05 ppb/h to 2.09 ppb/h, respectively, with the full consideration of the halogen processes in the CMAQ model. On the contrary, $D(O_x)$ decreased from 1.12 ppb/h to 0.97 ppb/h due to the limited contribution of O_3 destruction by halogen radicals. Consequently, $P(O_x)$ increased from 3.08 ppb/h to 3.33 ppb/h. The enhanced $F(O_x)$ of 0.09 ppb/h with decreased $D(O_x)$ of 0.15 ppb/h contribute to the increase in $P(O_x)$ of 0.25 ppb/h. Consistent results were observed at the Olympic Park and Mt. Taehwa stations (as shown in Figs. 5a and 5b).

On the other hand, the $F(O_x)$ decreased by 0.03 ppb/h, while both $D(O_x)$ and $P(O_x)$ increased by 0.12 ppb/h and 0.14 ppb/h, respectively, over the ocean (refer to Fig. 7b and Table 8). This may be caused by the halogen-related losses in $D(O_x)$ (caused mainly by IO+ HO_2 reaction), significantly contributing to the O_3 destruction. This indicates that the mixing ratios

https://doi.org/10.5194/egusphere-2025-23
Preprint. Discussion started: 21 January 2025

of O_3 tend to decrease in the presence of iodine radicals over the ocean areas. This is also in line with the case of the Bangnyung station, shown in Fig. 5c.

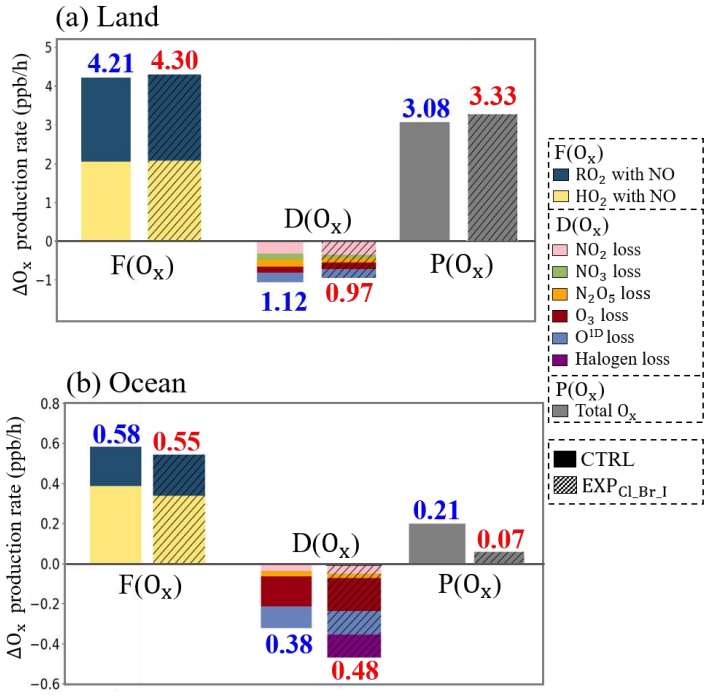

Figure 7. The stacked bar graphs represent O_x formation rate ($F(O_x)$), destruction rate ($D(Ox)$), and production rate ($P(O_x)$) in the CTRL (plain bars) and $EXP_{Cl\_Br\_I}$ (hatched bars) simulations over the (a) land and (b) ocean areas, respectively, during the period of KORUS-AQ campaign. Individual reactions contributing to $F(O_x)$ and $D(O_x)$ are indicated by the bar colors.

https://doi.org/10.5194/egusphere-2025-23
Preprint. Discussion started: 21 January 2025

Table 8. Averaged budget for O_x formation rates ($F(O_x)$), O_x destruction rates ($D(O_x)$), and O_x production rates ($P(O_x)$) calculated from the CTRL and $EXP_{Cl\_Br\_I}$ simulations during the period of KORUS-AQ campaign.

	Land		Ocean	
	CTRL	**$EXP_{Cl\_Br\_I}$**	**CTRL**	**$EXP_{Cl\_Br\_I}$**
O_x Formation: $F(O_x)$				
$RO_2 + NO$	2.16	2.21	0.20	0.21
$HO_2 + NO$	2.05	2.09	0.39	0.34
Total $F(O_x)$	4.21	4.30	0.58	0.55
O_x Destruction: $D(O_x)$				
NO_2 loss[1]	0.33	0.35	0.05	0.04
NO_3 loss[2]	0.17	0.09	< 0.01	< 0.01
N_2O_5 loss[3]	0.20	0.12	0.03	0.02
O_3 loss[4]	0.26	0.24	0.13	0.12
O^{1D} loss[5]	0.16	0.17	0.18	0.17
Halogen loss[6]	0	0.01	0	0.12
Total $D(O_x)$	1.12	0.97	0.38	0.48
Total O_x production: $P(O_x)$				
$P(O_x) = F(O_x) - D(O_x)$	3.08	3.33	0.21	0.07

NO_2 loss[1]= NO_2+RO_2 and NO_2+OH
NO_3 loss[2]= NO_3+VOC
N_2O_5 loss[3]= Heterogeneous reaction of N_2O_5
O_3 loss[4]= O_3 + OH, O_3 + VOC, and O_3 + HO_2
O^{1D} loss[5]= O^{1D}+H_2O
Halogen loss[6]= ClO + O_3, NO_2, and O^{3P}; Cl + O_3; BrO + OH; XO + HO_2; XO + XO (where X denotes Cl, Br, and I)

3.3 Impacts of halogen chemistry on atmospheric species

Figure 8 summarizes the impacts of halogen processes on the mixing ratios of key atmospheric species over/around the Korean peninsula. The mixing ratios of hydroxyl radicals (OH) and hydroperoxyl radicals (HO_2) increased by ~0.002 ppt (2.2%) and ~0.13 ppt (1.6%), respectively, when including the chlorine processes (i.e., EXP_{Cl} - CTRL). This is due to the fact that the chlorine radicals in the atmosphere substitute the role of OH radicals. In other words, chlorine radicals actively react with VOCs. Thus, the VOC mixing ratios decreased by 0.39 ppb (1.0%) due to the active VOC oxidation by Cl radicals. Formaldehyde (HCHO), an intermediate product of VOC oxidation, increased by 0.02 ppb (1.1%) due to the enhanced

https://doi.org/10.5194/egusphere-2025-23
Preprint. Discussion started: 21 January 2025

rates of the VOC oxidations by Cl radicals. The NO_x mixing ratios also increased by ~0.26 ppb (2.6%). Higher levels of NO_x may be due to the elevated levels of $ClNO_2$, which is a precursor of NO_x in the atmosphere.

We also explored the impacts of bromine processes (i.e., $EXP_{Cl\_Br} - EXP_{Cl}$). The mixing ratios of OH, HO_2, and HCHO further increased by ~0.001 ppt (1.1%), ~0.03 ppt (0.4%), and ~0.01 ppb (0.5%), respectively. These patterns appear to be similar to those in the chlorine case.

The effects of iodine chemistry (i.e., $EXP_{Cl\_Br\_I} - EXP_{Cl\_Br}$) revealed that OH mixing ratios increased by 0.004 ppt (3.1%). However, the mixing ratios of HO_2 decreased by 0.32 ppt (3.8%). This may be due to the complicated interactions of the following reactions: (i) $IO + O_3 \rightarrow IO$; (ii) $IO + HO_2 \rightarrow HOI$; (iii) $HOI \xrightarrow{hv} I + OH$ (null cycle: $O_3 + HO_2 \rightarrow 2OH + O_2$). Such patterns are prevalent over remote ocean areas affected by iodine chemistry. The levels of HCHO and VOCs remain almost unchanged due to the fact that iodine radicals do not strongly participate in the reactions with VOCs. The NO_x levels increased slightly by ~0.03 ppb (0.3%) on land and decreased by ~0.03 ppb (4.8%) over ocean areas, which is in line with findings from the previous study (Mahajan et al., 2021).

Collectively, the influence of the full halogen chemistries (i.e., $EXP_{Cl\_Br\_I} - CTRL$) shows that the OH mixing ratios increased significantly by 0.007 ppt (5.5%), while the HO_2 mixing ratios decreased by 0.45 ppt (5.4%) over ocean areas. These patterns are quite similar to those observed in the GEOS-Chem modeling study (Stone et al., 2018). The mixing ratios of HCHO and NO_x increased by ~0.03 ppb (1.6%) and ~0.29 ppb (2.9%) over the land. On the contrary, the mixing ratios of VOCs and NO_x decreased by ~0.71 ppb (5.9%) and ~0.05 ppb (7.8%) over the ocean areas, respectively.

In addition, elevated oxidant capacity in the simulation of $EXP_{Cl\_Br\_I}$ results in enhancements in the concentrations of sulfate by 0.05 $\mu g \cdot m^{-3}$ (1.5%) and secondary organic

https://doi.org/10.5194/egusphere-2025-23
Preprint. Discussion started: 21 January 2025

aerosols by 0.14 $\mu g \cdot m^{-3}$ (1.8%). However, concentrations of nitrate and ammonium decreased by ~1.60 $\mu g \cdot m^{-3}$ (29.4%) and ~0.55 $\mu g \cdot m^{-3}$ (5.0%), respectively, as shown in Fig. S6. This resulted from using smaller uptake coefficient for N_2O_5 (refer to Fig. S3), which suppresses NH_4NO_3 formation. As a result, $PM_{2.5}$ levels decreased from 21.59 $\mu g \cdot m^{-3}$ to 20.63 $\mu g \cdot m^{-3}$ (10.5%) over the Korean Peninsula during the KORUS-AQ campaign.

https://doi.org/10.5194/egusphere-2025-23
Preprint. Discussion started: 21 January 2025

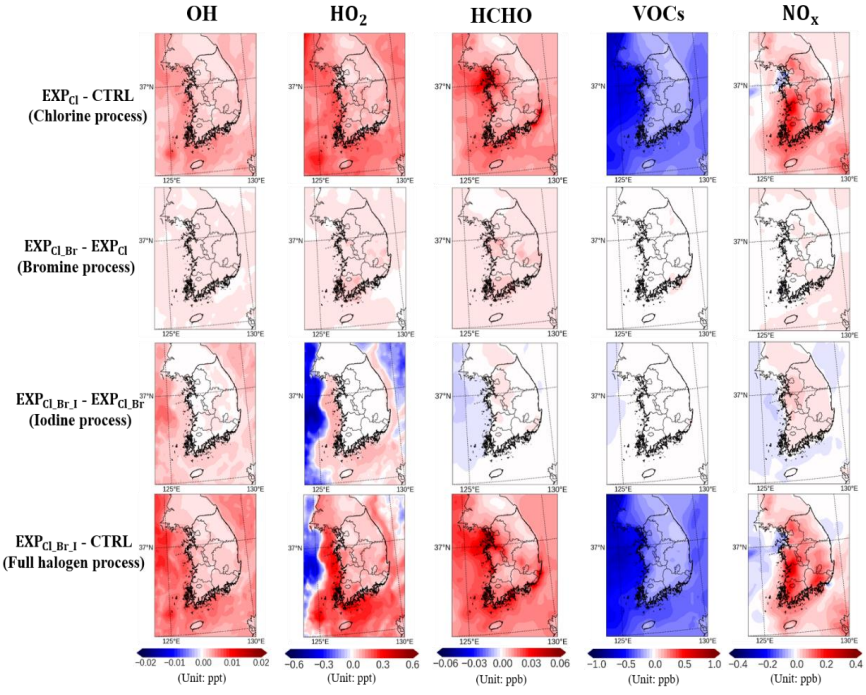

Figure 8. Summaries of the impacts of chlorine processes (EXP_{Cl} – CTRL), bromine processes (EXP_{Cl_Br} – EXP_{Cl}), iodine processes ($EXP_{Cl\_Br\_I}$ – EXP_{Cl_Br}), and full halogen processes ($EXP_{Cl\_Br\_I}$ – CTRL) on the mixing ratios of OH, HO_2, HCHO, VOCs, and NO_x, respectively, during the period of KORUS-AQ campaign.

4. Summary and Conclusions

To investigate the impacts of halogen chemistry over the Korean peninsula, we attempted to incorporate the halogen processes into the CMAQ modeling system. First, we estimated anthropogenic emissions of HCl, Cl_2, HBr, and Br_2 from five main sectors (such as industry, residential areas, power plants, solid waste incineration, and others). The anthropogenic emissions for HCl, Cl_2, HBr, and Br_2 are estimated to be 5,989.6, 450.8, 460.8, and 240.8 $Mg \cdot yr^{-1}$ over our research domain, respectively. Second, we also estimated emissions of natural halocarbons and inorganic bromine and iodine (Br_2, I, and HOI), based on the

https://doi.org/10.5194/egusphere-2025-23
Preprint. Discussion started: 21 January 2025

information derived from the GOCI sensor. Finally, we embedded halogen chemical reactions (58 chlorine reactions, 64 bromine reactions, and 55 iodine reactions) into the CMAQ model.

We then tested the model performances in terms of the mixing ratios of $ClNO_2$ during the period of the KORUS-AQ campaign at two supersites in South Korea. The $EXP_{Cl\_Br\_I}$ simulation exhibited the best performance in terms of the mixing ratios of $ClNO_2$. With the $EXP_{Cl\_Br\_I}$ simulation, the IOA increased from 0.41 to 0.66 at the Olympic Park station, and 0.40 to 0.59 at the Mt.Taehwa station. Meanwhile, the MB decreased from -85.97 to 30.79 at the Olympic Park station, and -159.36 ppt to -25.07 ppt at the Mt.Taehwa station. This is because the four following halogen reactions considered in this study contributed to better $ClNO_2$ simulations: (i) $ClO + ClO \rightarrow Cl_2$; (ii) $HOBr + Cl^- \rightarrow BrCl$; (iii) different parameterization of γ_{N2O5}; and (iv) $2NO_2 + Cl^- \rightarrow ClNO + NO_3^-$.

Our study further emphasized the significant influences of individual halogen processes on O_3 mixing ratios over South Korea. The average mixing ratios of O_3 increased by ~ 0.21 ppb (0.5%) over land areas due to the impacts of chlorine and bromine processes. On the contrary, the O_3 mixing ratios decreased by ~0.69 ppb (1.2%) over ocean areas due to iodine processes. In addition, we quantitatively calculated the O_x budget. The net O_x production rate ($P(O_x)$) increased from 3.08 to 3.32 ppb/h over the land areas and decreased from 0.21 to 0.07 ppb/h over the ocean areas with the simulation of the $EXP_{Cl\_Br\_I}$.

Finally, we further explored the impacts of full halogen processes on the atmospheric composition. Compared with the CTRL simulation, the mixing ratios of HCHO and NO_x increased by ~0.03 ppb (1.6%) and ~0.29 ppb (2.9%) over the land, respectively. On the other hand, the mixing ratios of HO_2 and VOCs decreased by ~0.45 ppt (5.3%) and ~0.71 ppb (5.9%) over the ocean areas, respectively, during the period of the KORUS-AQ campaign.

In conclusion, we believe that we successfully incorporated comprehensive halogen processes into the CMAQ modeling system. Although our study showed good agreement with

https://doi.org/10.5194/egusphere-2025-23
Preprint. Discussion started: 21 January 2025

observations, this is only in terms of a few species such as $ClNO_2$ and Cl_2. There are still lack of information such as insufficient observational data, uncertainties in uptake coefficients of reactive halogen species, and uncertainties in the reaction rates of these species. Obviously, further studies are necessary in the future to investigate these uncertainties in the halogen chemistry.

https://doi.org/10.5194/egusphere-2025-23
Preprint. Discussion started: 21 January 2025

Code and data availability

After user registration, the WRF model 3.8.1 (https://doi.org/10.5065/D6MK6B4K, WRF User Page, 2024) and CMAQ v5.2.1 (https://doi.org/10.5281/zenodo.1079909, US EPA Office of Research and Development, 2015) are available from web page. The observation data we used can be accessed at https://www-air.larc.nasa.gov/cgi-bin/ArcView/korusaq?GROUND-NIER-OLYMPIC-PARK=1 (NASA, 2019).

Author contributions

Conceptualization: KK, CHS, and KMH. Writing: KK, CHS, and KMH. Experimental design: KK, CHS, KMH, GY, and RB. Supervision: CHS. Validation: KK and CHS. Analysis: KK. Data curation: SK. All authors contributed to this paper for publication.

Competing interests

At least one of the (co-)authors is a member of the editorial board of *Atmospheric Chemistry and Physics*. The authors declare that they have no known competing financial interests or personal relationships that could have appeared to influence the work reported in this paper.

Acknowledgment

This work was supported by the National Research Foundation of Korea (NRF) grand funded by the Korea government (MSIT) (grant number: 2021R1A2C1006660).

https://doi.org/10.5194/egusphere-2025-23
Preprint. Discussion started: 21 January 2025

References

Abbatt, J. and Waschewsky, G.: Heterogeneous interactions of HOBr, HNO3, O3, and NO2 with deliquescent NaCl aerosols at room temperature, J. Phys. Chem. A, 102, 3719-3725, https://doi.org/10.1021/jp980932d, 1998.

Ammann, M., Cox, R. A., Crowley, J., Jenkin, M. E., Mellouki, A., Rossi, M. J., Troe, J., and Wallington, T. J.: Evaluated kinetic and photochemical data for atmospheric chemistry: Volume VI–heterogeneous reactions with liquid substrates, Atmos. Chem. Phys., 13, 8045-8228, https://doi.org/10.5194/acp-13-8045-2013, 2013.

Baklanov, A., Chesnokov, E., and Chichinin, A.: Rate constants for the reactions of molecular iodine with Cl, SiCl3, and SiH3 at 298 K, International Journal of Chemical Kinetics, 29, 25-33, https://doi.org/10.1002/(SICI)1097-4601(1997)29:1<25::AID-KIN4>3.0.CO;2-N, 1997.

Bedjanian, Y., Le Bras, G., and Poulet, G.: Rate constants for the reactions I+ OClO, I+ ClO, Cl+ I2, and Cl+ IO and heat of formation of IO radicals, J. Phys. Chem., 100, 15130-15136, https://doi.org/10.1021/jp960696b, 1996.

Bertram, T. and Thornton, J.: Toward a general parameterization of N2O5 reactivity on aqueous particles: the competing effects of particle liquid water, nitrate and chloride, Atmos. Chem. Phys., 9, 8351-8363, https://doi.org/10.5194/acp-9-8351-2009, 2009.

Burkholder, J., Sander, S., Abbatt, J., Barker, J., Cappa, C., Crounse, J., Dibble, T., Huie, R., Kolb, C., and Kurylo, M.: Chemical kinetics and photochemical data for use in atmospheric studies; evaluation number 19, Nasa panel for data evaluation technical report, 19-5, https://jpldataeval.jpl.nasa.gov/pdf/NASA-JPL%20Evaluation%2019-5.pdf, 2020.

Byun, D. and Schere, K. L.: Review of the governing equations, computational algorithms, and other components of the Models-3 Community Multiscale Air Quality (CMAQ) modeling system, Appl. Mech. Rev., 59, 51-77, https://doi.org/10.1115/1.2128636, 2006.

Caram, C., Szopa, S., Cozic, A., Bekki, S., Cuevas, C. A., and Saiz-Lopez, A.: Sensitivity of tropospheric ozone to halogen chemistry in the chemistry–climate model LMDZ-INCA vNMHC, Geosci. Model Dev., 16, 4041-4062, https://doi.org/10.5194/gmd-16-4041-2023, 2023.

Carter, W. P.: Development of the SAPRC-07 chemical mechanism, Atmos. Environ., 44, 5324-5335, https://doi.org/10.1016/j.atmosenv.2010.01.026, 2010.

Chang, W. L., Brown, S. S., Stutz, J., Middlebrook, A. M., Bahreini, R., Wagner, N. L., Dubé, W. P., Pollack, I. B., Ryerson, T. B., and Riemer, N.: Evaluating N2O5 heterogeneous hydrolysis parameterizations for CalNex 2010, J. Geophys. Res., 121, 5051-5070, https://doi.org/10.1002/2015JD024737, 2016.

Chen, Q., Xia, M., Peng, X., Yu, C., Sun, P., Li, Y., Liu, Y., Xu, Z., Xu, Z., and Wu, R.: Large daytime molecular chlorine missing source at a suburban site in East China, J. Geophys. Res., 127, e2021JD035796, https://doi.org/10.1029/2021JD035796, 2022.

Clyne, M. and Cruse, H.: Atomic resonance fluorescence spectrometry for rate constants of rapid bimolecular reactions. Part 1.—Reactions O+ NO 2, Cl+ ClNO, Br+ ClNO, J. Chem. Soc. Faraday Trans., 68, 1281-1299, https://doi.org/10.1039/F29726801281, 1972.

Deiber, G., George, C., Le Calvé, S., Schweitzer, F., and Mirabel, P.: Uptake study of ClONO 2 and BrONO 2 by Halide containing droplets, Atmos. Chem. Phys., 4, 1291-1299, https://doi.org/10.5194/acp-4-1291-2004, 2004.

Deng, S., Shi, Y., Liu, Y., Zhang, C., Wang, X., Cao, Q., Li, S., and Zhang, F.: Emission characteristics of Cd, Pb and Mn from coal combustion: Field study at coal-fired power plants in China, Fuel Processing Technology, 126, 469-475, https://doi.org/10.1016/j.fuproc.2014.06.009, 2014.

Edwards, P. M. and Young, C. J.: Primary Radical Effectiveness: Do the Different Chemical Reactivities of Hydroxyl and Chlorine Radicals Matter for Tropospheric Oxidation?, ACS ES&T Air, https://doi.org/10.1021/acsestair.3c00108, 2024.

Evans, M. J. and Jacob, D. J.: Impact of new laboratory studies of N2O5 hydrolysis on global model budgets of tropospheric nitrogen oxides, ozone, and OH, Geophys. Res. Lett., 32, https://doi.org/10.1029/2005GL022469, 2005.

Fan, S. and Li, Y.: The impacts of marine-emitted halogens on OH radicals in East Asia during summer, Atmos. Chem. Phys., 22, 7331-7351, https://doi.org/10.5194/acp-22-7331-2022, 2022.

Fernandez, R. P., Salawitch, R., Kinnison, D. E., Lamarque, J.-F., and Saiz-Lopez, A.: Bromine partitioning in the tropical tropopause layer: implications for stratospheric injection, Atmos. Chem. Phys., 14, 13391-13410, https://doi.org/10.5194/acp-14-13391-2014, 2014.

Gantt, B., Sarwar, G., Xing, J., Simon, H., Schwede, D., Hutzell, W. T., Mathur, R., and Saiz-Lopez, A.: The impact of iodide-mediated ozone deposition and halogen chemistry on surface ozone concentrations across the continental United States, Environ. Sci. Technol., 51, 1458-1466, https://doi.org/10.1021/acs.est.6b03556, 2017.

https://doi.org/10.5194/egusphere-2025-23
Preprint. Discussion started: 21 January 2025

Giri, B. R., Farooq, A., Szőri, M., and Roscoe, J. M.: The kinetics of the reactions of Br atoms with the xylenes: an experimental and theoretical study, Phys. Chem. Chem. Phys., 24, 4843-4858, https://doi.org/10.1039/D1CP03740D, 2022.

Guenther, A., Jiang, X., Heald, C. L., Sakulyanontvittaya, T., Duhl, T. a., Emmons, L., and Wang, X.: The Model of Emissions of Gases and Aerosols from Nature version 2.1 (MEGAN2. 1): an extended and updated framework for modeling biogenic emissions, Geosci. Model Dev., 5, 1471-1492, https://doi.org/10.5194/gmd-5-1471-2012, 2012.

Herrmann, M., Schöne, M., Borger, C., Warnach, S., Wagner, T., Platt, U., and Gutheil, E.: Ozone depletion events in the Arctic spring of 2019: a new modeling approach to bromine emissions, Atmos. Chem. Phys., 22, 13495-13526, https://doi.org/10.5194/acp-22-13495-2022, 2022.

Huang, Y., Lu, X., Fung, J. C., Sarwar, G., Li, Z., Li, Q., Saiz-Lopez, A., and Lau, A. K.: Effect of bromine and iodine chemistry on tropospheric ozone over Asia-Pacific using the CMAQ model, Chemosphere, 262, 127595, https://doi.org/10.1016/j.chemosphere.2020.127595, 2021.

Hutzell, W., Luecken, D., Appel, K., and Carter, W.: Interpreting predictions from the SAPRC07 mechanism based on regional and continental simulations, Atmos. Environ., 46, 417-429, https://doi.org/10.1016/j.atmosenv.2011.09.030, 2012.

Jeong, D., Seco, R., Gu, D., Lee, Y., Nault, B. A., Knote, C. J., Mcgee, T., Sullivan, J. T., Jimenez, J. L., and Campuzano-Jost, P.: Integration of airborne and ground observations of nitryl chloride in the Seoul metropolitan area and the implications on regional oxidation capacity during KORUS-AQ 2016, Atmos. Chem. Phys., 19, 12779-12795, https://doi.org/10.5194/acp-19-12779-2019, 2019.

Jiang, J., Hao, J., Wu, Y., Streets, D. G., Duan, L., and Tian, H.: Development of mercury emission inventory from coal combustion in China, Environ. Sci., 26, 34-39, https://doi.org/10.13227/j.hjkx.2005.02.007, 2005 (in Chinese).

Jo, H.-Y., Park, J., Heo, G., Lee, H.-J., Jeon, W., Kim, J.-M., Kim, S., Kim, J.-K., Liu, Y., and Liu, P.: Interpretation of the effects of anthropogenic chlorine on nitrate formation over northeast Asia during KORUS-AQ 2016, Sci. Total Environ., 164920, https://doi.org/10.1016/j.scitotenv.2023.164920, 2023.

Keefer, R. and Andrews, L.: The interaction of bromine with benzene and certain of its derivatives, J. Am. Chem. Soc., 72, 4677-4681, https://doi.org/10.1021/ja01166a091, 1950.

Khamaganov, V. and Crowley, J.: Rate coefficients for the reactions CH3+ Br2 (224–358 K), CH3CO+ Br2 (228 and 298 K), and Cl+ Br2 (228 and 298 K), International Journal of Chemical Kinetics, 42, 575-585, https://doi.org/10.1002/kin.20505, 2010.

Kim, H., Park, R. J., Kim, S., Jeong, J. I., Jeong, D., Fu, X., and Cho, S.: Effect of nitryl chloride chemistry on air quality in South Korea during the KORUS-AQ campaign, Atmos. Environ., 312, 120045, https://doi.org/10.1016/j.atmosenv.2023.120045, 2023.

Kim, W., Moon, J.-E., Park, Y.-J., and Ishizaka, J.: Evaluation of chlorophyll retrievals from Geostationary Ocean color imager (GOCI) for the north-east Asian region, Remote Sens. Environ., 184, 482-495, https://doi.org/10.1016/j.rse.2016.07.031, 2016.

Li, Q., Zhang, L., Wang, T., Tham, Y. J., Ahmadov, R., Xue, L., Zhang, Q., and Zheng, J.: Impacts of heterogeneous uptake of dinitrogen pentoxide and chlorine activation on ozone and reactive nitrogen partitioning: improvement and application of the WRF-Chem model in southern China, Atmos. Chem. Phys., 16, 14875-14890, https://doi.org/10.5194/acp-16-14875-2016, 2016.

Li, Q., Fu, X., Peng, X., Wang, W., Badia, A., Fernandez, R. P., Cuevas, C. A., Mu, Y., Chen, J., and Jimenez, J. L.: Halogens enhance haze pollution in China, Environ. Sci. Technol., 55, 13625-13637, https://doi.org/10.1021/acs.est.1c01949, 2021.

Liss, P. S., Marandino, C. A., Dahl, E. E., Helmig, D., Hintsa, E. J., Hughes, C., Johnson, M. T., Moore, R. M., Plane, J. M., and Quack, B.: Short-lived trace gases in the surface ocean and the atmosphere, Ocean-atmosphere Interactions of Gases and Particles, 1-54, https://doi.org/10.1007/978-3-642-25643-1_1, 2014.

Liu, L., Bei, N., Wu, J., Liu, S., Zhou, J., Li, X., Yang, Q., Feng, T., Cao, J., and Tie, X.: Effects of stabilized Criegee intermediates (sCIs) on sulfate formation: a sensitivity analysis during summertime in Beijing–Tianjin–Hebei (BTH), China, Atmos. Chem. Phys., 19, 13341-13354, https://doi.org/10.5194/acp-19-13341-2019, 2019.

Liu, T. and Abbatt, J. P.: An experimental assessment of the importance of S (IV) oxidation by hypohalous acids in the marine atmosphere, Geophys. Res. Lett., 47, e2019GL086465, https://doi.org/10.1029/2019GL086465, 2020.

Liu, Y., Fan, Q., Chen, X., Zhao, J., Ling, Z., Hong, Y., Li, W., Chen, X., Wang, M., and Wei, X.: Modeling the impact of chlorine emissions from coal combustion and prescribed waste incineration on tropospheric ozone formation in China, Atmos. Chem. Phys., 18, 2709-2724, https://doi.org/10.5194/acp-18-2709-2018, 2018.

Mahajan, A. S., Li, Q., Inamdar, S., Ram, K., Badia, A., and Saiz-Lopez, A.: Modelling the impacts of iodine chemistry on the northern Indian Ocean marine boundary layer, Atmos. Chem. Phys., 21, 8437-8454,

https://doi.org/10.5194/egusphere-2025-23
Preprint. Discussion started: 21 January 2025

https://doi.org/10.5194/acp-21-8437-2021, 2021.
McDuffie, E. E., Fibiger, D. L., Dubé, W. P., Lopez-Hilfiker, F., Lee, B. H., Thornton, J. A., Shah, V., Jaeglé, L., Guo, H., and Weber, R. J.: Heterogeneous N2O5 uptake during winter: Aircraft measurements during the 2015 WINTER campaign and critical evaluation of current parameterizations, J. Geophys. Res., 123, 4345-4372, https://doi.org/10.1002/2018JD028336, 2018.
O'Reilly, J. E. and Werdell, P. J.: Chlorophyll algorithms for ocean color sensors-OC4, OC5 & OC6, Remote Sens. Environ., 229, 32-47, https://doi.org/10.1016/j.rse.2019.04.021, 2019.
Park, M.-O., Shin, W.-C., Son, Y.-B., and Noh, T.-G.: Spatial Variability of in situ and GOCI and MODIS Chlorophyll and CDOM in Summer at the East Sea, Journal of the Korean Society of Marine Environment & Safety, 21, 327-338, https://doi.org/10.7837/kosomes.2015.21.4.327, 2015.
Parrella, J., Jacob, D. J., Liang, Q., Zhang, Y., Mickley, L. J., Miller, B., Evans, M., Yang, X., Pyle, J., and Theys, N.: Tropospheric bromine chemistry: implications for present and pre-industrial ozone and mercury, Atmos. Chem. Phys., 12, 6723-6740, https://doi.org/10.5194/acp-12-6723-2012, 2012.
PENG, B.-x. and WU, D.-s.: Distribution and content of bromine in Chinese coals, Journal of Fuel Chemistry and Technology, 42, 769-773, https://doi.org/10.1016/S1872-5813(14)60034-7, 2014.
Peng, X., Wang, T., Wang, W., Ravishankara, A., George, C., Xia, M., Cai, M., Li, Q., Salvador, C. M., and Lau, C.: Photodissociation of particulate nitrate as a source of daytime tropospheric Cl2, Nat. Commun., 13, 939, https://doi.org/10.6084/m9.figshare.17099252, 2022.
Pratte, P. and Rossi, M. J.: The heterogeneous kinetics of HOBr and HOCl on acidified sea salt and model aerosol at 40–90% relative humidity and ambient temperature, Phys. Chem. Chem. Phys., 8, 3988-4001, https://doi.org/10.1039/B604321F, 2006.
Qiu, X., Ying, Q., Wang, S., Duan, L., Wang, Y., Lu, K., Wang, P., Xing, J., Zheng, M., and Zhao, M.: Significant impact of heterogeneous reactions of reactive chlorine species on summertime atmospheric ozone and free-radical formation in north China, Sci. Total Environ., 693, 133580, https://doi.org/10.1016/j.scitotenv.2019.133580, 2019a.
Qiu, X., Ying, Q., Wang, S., Duan, L., Zhao, J., Xing, J., Ding, D., Sun, Y., Liu, B., and Shi, A.: Modeling the impact of heterogeneous reactions of chlorine on summertime nitrate formation in Beijing, China, Atmos. Chem. Phys., 19, 6737-6747, https://doi.org/10.5194/acp-19-6737-2019, 2019b.
Read, K. A., Mahajan, A. S., Carpenter, L. J., Evans, M. J., Faria, B. V., Heard, D. E., Hopkins, J. R., Lee, J. D., Moller, S. J., and Lewis, A. C.: Extensive halogen-mediated ozone destruction over the tropical Atlantic Ocean, Nature, 453, 1232-1235, https://doi.org/10.1038/nature07035, 2008.
Riedel, T., Bertram, T., Ryder, O., Liu, S., Day, D., Russell, L., Gaston, C., Prather, K., and Thornton, J.: Direct N 2 O 5 reactivity measurements at a polluted coastal site, Atmos. Chem. Phys., 12, 2959-2968, https://doi.org/10.5194/acp-12-2959-2012, 2012a.
Riedel, T. P., Bertram, T. H., Crisp, T. A., Williams, E. J., Lerner, B. M., Vlasenko, A., Li, S.-M., Gilman, J., De Gouw, J., and Bon, D. M.: Nitryl chloride and molecular chlorine in the coastal marine boundary layer, Environ. Sci. Technol., 46, 10463-10470, https://doi.org/10.1021/es204632r, 2012b.
Riemer, N., Vogel, H., Vogel, B., Schell, B., Ackermann, I., Kessler, C., and Hass, H.: Impact of the heterogeneous hydrolysis of N2O5 on chemistry and nitrate aerosol formation in the lower troposphere under photosmog conditions, J. Geophys. Res. -Atmos., 108, https://doi.org/10.1029/2002JD002436, 2003.
Roberts, J. M., Osthoff, H. D., Brown, S. S., Ravishankara, A., Coffman, D., Quinn, P., and Bates, T.: Laboratory studies of products of N2O5 uptake on Cl− containing substrates, Geophys. Res. Lett., 36, https://doi.org/10.1029/2009GL040448, 2009.
Saiz-Lopez, A., Fernandez, R. P., Ordóñez, C., Kinnison, D. E., Gómez Martín, J., Lamarque, J.-F., and Tilmes, S.: Iodine chemistry in the troposphere and its effect on ozone, Atmos. Chem. Phys., 14, 13119-13143, https://doi.org/10.5194/acp-14-13119-2014, 2014.
Saiz-Lopez, A., Lamarque, J.-F., Kinnison, D. E., Tilmes, S., Ordóñez, C., Orlando, J. J., Conley, A. J., Plane, J., Mahajan, A. S., and Sousa Santos, G.: Estimating the climate significance of halogen-driven ozone loss in the tropical marine troposphere, Atmos. Chem. Phys., 12, 3939-3949, https://doi.org/10.5194/acp-12-3939-2012, 2012.
Sander, S., Friedl, R., Golden, D., Kurylo, M., Moortgat, G., Wine, P., Ravishankara, A., Kolb, C., Molina, M., and Finlyason-Pitts, B.: Chemical kinetics and photochemical data for use in atmospheric studies: Evaluation number 15, Pasadena, CA: Jet Propulsion Laboratory, California Institute of Technology2010.
Sarwar, G., Simon, H., Bhave, P., and Yarwood, G.: Examining the impact of heterogeneous nitryl chloride production on air quality across the United States, Atmos. Chem. Phys., 12, 6455-6473, https://doi.org/10.5194/acp-12-6455-2012, 2012.
Sarwar, G., Gantt, B., Schwede, D., Foley, K., Mathur, R., and Saiz-Lopez, A.: Impact of enhanced ozone deposition and halogen chemistry on tropospheric ozone over the Northern Hemisphere, Environ. Sci. Technol., 49, 9203-9211, https://doi.org/10.1021/acs.est.5b01657, 2015.

https://doi.org/10.5194/egusphere-2025-23
Preprint. Discussion started: 21 January 2025

Sarwar, G., Gantt, B., Foley, K., Fahey, K., Spero, T. L., Kang, D., Mathur, R., Foroutan, H., Xing, J., and Sherwen, T.: Influence of bromine and iodine chemistry on annual, seasonal, diurnal, and background ozone: CMAQ simulations over the Northern Hemisphere, Atmos. Environ., 213, 395-404, https://doi.org/10.1016/j.atmosenv.2019.06.020, 2019.

Sherwen, T., Evans, M., Carpenter, L., Andrews, S., Lidster, R., Dix, B., Koenig, T., Sinreich, R., Ortega, I., and Volkamer, R.: Iodine's impact on tropospheric oxidants: a global model study in GEOS-Chem, Atmos. Chem. Phys., 16, 1161-1186, https://doi.org/10.5194/acp-16-1161-2016, 2016.

Simpson, W. R., Brown, S. S., Saiz-Lopez, A., Thornton, J. A., and von Glasow, R.: Tropospheric halogen chemistry: Sources, cycling, and impacts, Chem. Rev., 115, 4035-4062, https://doi.org/10.1021/cr5006638, 2015.

Skamarock, W. C., Klemp, J. B., Dudhia, J., Gill, D. O., Barker, D. M., Duda, M. G., Huang, X.-Y., Wang, W., and Powers, J. G.: A description of the advanced research WRF version 3, NCAR technical note, 475, 10.5065, https://doi.org/10.5065/D68S4MVH, 2008.

Slusher, D. L., Huey, L. G., Tanner, D. J., Flocke, F. M., and Roberts, J. M.: A thermal dissociation–chemical ionization mass spectrometry (TD-CIMS) technique for the simultaneous measurement of peroxyacyl nitrates and dinitrogen pentoxide, J. Geophys. Res., 109, https://doi.org/10.1029/2004JD004670, 2004.

Stone, D., Sherwen, T., Evans, M. J., Vaughan, S., Ingham, T., Whalley, L. K., Edwards, P. M., Read, K. A., Lee, J. D., and Moller, S. J.: Impacts of bromine and iodine chemistry on tropospheric OH and HO 2: comparing observations with box and global model perspectives, Atmos. Chem. Phys., 18, 3541-3561, https://doi.org/10.5194/acp-18-3541-2018, 2018.

von Glasow, R. and Crutzen, P. J.: Tropospheric halogen chemistry, Treatise on Geochemistry, 4, 347, 2003.

Wang, X., Wang, H., Xue, L., Wang, T., Wang, L., Gu, R., Wang, W., Tham, Y. J., Wang, Z., and Yang, L.: Observations of N2O5 and ClNO2 at a polluted urban surface site in North China: High N2O5 uptake coefficients and low ClNO2 product yields, Atmos. Environ., 156, 125-134, https://doi.org/10.1016/j.atmosenv.2017.02.035, 2017.

Wiedinmyer, C., Akagi, S., Yokelson, R. J., Emmons, L., Al-Saadi, J., Orlando, J., and Soja, A.: The Fire INventory from NCAR (FINN): A high resolution global model to estimate the emissions from open burning, Geosci. Model Dev., 4, 625-641, https://doi.org/10.5194/gmd-4-625-2011, 2011.

Woo, J.-H., Kim, Y., Kim, H.-K., Choi, K.-C., Eum, J.-H., Lee, J.-B., Lim, J.-H., Kim, J., and Seong, M.: Development of the CREATE inventory in support of integrated climate and air quality modeling for Asia, Sustainability, 12, 7930, https://doi.org/10.3390/su12197930, 2020.

Yi, X., Yin, S., Huang, L., Li, H., Wang, Y., Wang, Q., Chan, A., Traoré, D., Ooi, M. C. G., and Chen, Y.: Anthropogenic emissions of atomic chlorine precursors in the Yangtze River Delta region, China, Sci. Total Environ., 771, 144644, https://doi.org/10.1016/j.scitotenv.2020.144644, 2021.

Yu, C., Wang, Z., Xia, M., Fu, X., Wang, W., Tham, Y. J., Chen, T., Zheng, P., Li, H., and Shan, Y.: Heterogeneous N2O5 reactions on atmospheric aerosols at four Chinese sites: improving model representation of uptake parameters, Atmos. Chem. Phys., 20, 4367-4378, https://doi.org/10.5194/acp-20-4367-2020, 2020.